



Published in final edited form as:

*Nat Biomed Eng.* 2023 April ; 7(4): 405–423. doi:10.1038/s41551-021-00683-3.

## Wireless and battery-free technologies for neuroengineering

**Sang Min Won**<sup>#1</sup>, **Le Cai**<sup>#2</sup>, **Philipp Gutruf**<sup>2,3,4,\*</sup>, **John A. Rogers**<sup>5,6,7,8,9,10,11,12,13,\*</sup>

<sup>1</sup>Department of Electrical and Computer Engineering, Sungkyunkwan University, Suwon, 16419, South Korea.

<sup>2</sup>Biomedical Engineering, College of Engineering, The University of Arizona, Tucson, AZ, USA.

<sup>3</sup>Bio5 Institute and Department of Neurology, University of Arizona, Tucson, AZ, 85721, USA

<sup>4</sup>Department of Electrical and Computer Engineering, University of Arizona, Tucson, AZ 85721, USA.

<sup>5</sup>Department of Materials Science and Engineering, Northwestern University, Evanston, IL, USA.

<sup>6</sup>Center for Bio-Integrated Electronics, Northwestern University, Evanston, IL, USA.

<sup>7</sup>Department of Biomedical Engineering, Northwestern University, Evanston, IL, USA.

<sup>8</sup>Center for Advanced Molecular Imaging, Northwestern University, Evanston, IL, USA.

<sup>9</sup>Department of Mechanical Engineering, Northwestern University, Evanston, IL, USA.

<sup>10</sup>Department of Chemistry, Northwestern University, Evanston, IL, USA.

<sup>11</sup>Department of Neurological Surgery, Northwestern University, Evanston, IL, USA.

<sup>12</sup>Department of Electrical and Computer Engineering, Northwestern University, Evanston, IL, USA.

<sup>13</sup>Simpson Querrey Institute for BioNanotechnology, Northwestern University, Evanston, IL, USA.

# These authors contributed equally to this work.

### Abstract

Tethered optical, electrical and fluidic battery-powered devices that interface with neural tissue constrain or prevent subject motion, as well as social interactions, and prevent their long-term use in larger models, such as non-human primates, which inhabit complex environments, move over large distances and have high levels of manual dexterity. Here, we discuss recent advances in ultra-lightweight, miniaturized, wireless and battery-free devices that are fully implantable, with capabilities that match or exceed the performance of tethered and battery-powered alternatives, while bypassing their intrinsic limitations. These systems enable closed-loop applications that combine neural recordings and neurostimulation and include the long-lived delivery of therapeutic compounds and the real-time monitoring and treatment of abnormal physiological functions.

\*Corresponding author Correspondence to Philipp Gutruf or John A. Rogers jrogers@northwestern.edu; pgutruf@arizona.edu.  
Author Contributions

All authors contributed to writing the paper, revising it and approving the final version.

Competing interests

The authors declare no competing interests

## Editorial Summary

Recent advances in material science and neuroengineering serve as the foundations for lightweight, miniaturized and fully implantable wireless devices that interface with biological tissues for recording and stimulating neural activity, without the need for batteries or physical tethers.

---

Advances in electronic, optoelectronic and microfluidic interfaces with living biosystems serve as the foundations for the development of versatile tools capable of interrogating the central and peripheral nervous systems.<sup>1-5</sup> The implications for the field extend beyond their use in fundamental research and include approaches for the treatment of neurological disorders and diseases.<sup>6-11</sup> The most advanced devices currently approved for human use for deep brain stimulation, cochlear implants and cardiac pacemakers utilize rigid and comparatively large electronic modules electrically connected to metal electrodes that interface with neural cells. Despite their success in monitoring and ameliorating diverse neurological disorders and diseases, including depression, epilepsy, chronic pain, deafness, and Parkinson's disease, their limited modalities of operation and the mechanical mismatch between the tissues and the hardware represent areas where advances in neuroengineering can, in principle, facilitate intimate, long-lived neural interfaces with diverse operational modes. Recent progress in implantable neural interfaces qualitatively extend designs and capabilities of existing miniaturized systems, to support delivery of user-programmed optical,<sup>12-15</sup> chemical,<sup>14, 16-19</sup> and electrical stimuli<sup>20-23</sup> in real-time, with formats that require only minimally invasive implantation procedures and that offer stability in operation over extended periods of time. These implantable neural interfaces are distinct from (and potentially have complementary functions to) recently developed materials-based approaches, such as upconverting nanoparticles that convert incident near infrared illumination to visible light stimulus,<sup>1, 24, 25</sup> magnetic nanoparticles that transduce magnetic fields to mechanical, electrical and thermal stimuli,<sup>1, 26-28</sup> and ultrasound-based contrast agents capable of transiently opening the blood-brain barrier for the local delivery of therapeutic agents,<sup>29, 30</sup>. Here, we focus on engineered miniaturized systems that exploit schemes in wireless power transfer, communication and digital control that support broad applications in neuroscience studies, cardiac research and monitoring of organ function.<sup>31-33</sup>

Commonly used technologies rely on electrochemical power sources such as batteries and supercapacitors or on similarly large, bulky systems for energy harvesting,<sup>16, 34-39</sup> due partly to their technological maturity and widespread availability. Conventional rigid printed circuit boards typically serve as mounting sites for centimeter-scale electronic components for wireless transmission, physiological recording and control of stimulation. Devices that use these designs can however cause irritation, infections, motion artefacts, and reduced freedom of motion, particularly in small animal models such as mice, making size and weight of externalized devices<sup>16, 40-44</sup> key limiting parameters. Restrictions following from large formfactors also affect the precise interpretation of experimental data and in many cases preclude behavioral studies in real-life environments. Fully wireless, lightweight systems that are battery-free and adopt miniaturized form factors, configured for complete and long-term implantation, allow for continuous behavioral studies without requirements for human interaction.

This paper captures the latest technologies in wireless implantable devices and compares their designs and capabilities with those of traditional tethered and battery-powered systems. Material selections and engineering approaches for functional interfaces are discussed in the context of biocompatibility and hermeticity, wireless data communication and power transfer. Although embodiments of these technologies are highlighted as tools for fundamental neuroscience research and multifunctional neuroengineering in small animal models, the results also establish foundational methods and technologies for the translation to large animals and human subjects.

### Limitations of tethered systems.

Technologies that rely on physical tethers such as electrical wires, fiber optic cables or fluidic tubing are commonly used in neuroscience research and in medical systems, due in part to the simplicity and commodity nature of the component parts. For example, optogenetic stimulation and cell recordings to interrogate neural function in the brain are typically achieved using optical fiber technologies adapted from the telecommunications industry.<sup>45, 46</sup> Here, the fiber optic couples to an external light source, and creates an optical interface with a targeted region in the brain. The materials and geometric properties of the fiber and the light source determine the type of illumination<sup>47-51</sup>. Examples include angle-adjusted optical coupling into tapered fibers for selective neurostimulation,<sup>47</sup> multifunctional fibers for coordinated electrical recording, optogenetic stimulation and biological agent delivery<sup>48</sup>, and fiber-based photometers for stimulation and recording of fluorescence from genetically targeted Ca<sup>2+</sup> indicators<sup>49, 50, 52</sup> and fluorescent voltage reporters.<sup>51</sup> Other tethered systems utilize head-mounted electronics and/or cable assemblies in conjunction with implantable light sources and electrical/optical recording components. For instance, advanced platforms use micro-structured injectable needles with integrated microscale inorganic light-emitting diodes ( $\mu$ -ILEDs) and electrodes for multi-site recording and stimulation with spatial resolution on the cellular scale.<sup>53</sup> Others use miniaturized head-stage camera setups coupled with chronically implanted lenses for visualizing neural circuit dynamics with high spatial resolution.<sup>54, 55</sup> Such tether-based technologies, however, pose particular difficulties when interfacing with highly mobile areas like the spinal cord or peripheral nerves because of the need for fixation to mechanically stable parts of the anatomy such as the skull or to specialized orthosis.<sup>56</sup> Furthermore, the forces exerted on the implant by the tethers during natural motions, or associated with plugging and unplugging or unwinding of the cables, results in micro-motions between the rigid probes and the soft tissues that cause tissue damage and artefacts, leading to diminished chronic stability.<sup>57, 58</sup> Unrestrained animals often also attempt to remove or disconnect the cables, particularly with advanced interfaces that demand multichannel operation.<sup>59</sup>

The development of wireless, implantable recording and stimulation tools for long-term operation and robust, high fidelity interfaces with the central and peripheral nervous systems aims to increase the experimental reproducibility and to reduce interactions with the test subjects and environmental obstacles (Figure 1a). The advantages of wireless implants become apparent in comparative studies of fiber-tethered and battery-powered wireless optogenetic photometric devices. The data show, in many cases, that the tethers can significantly impede social behaviors and overall patterns of activity of the animals (Figure

1b, c).<sup>60</sup> In one set of experiments, compared with otherwise identical untethered subjects, mice with fiber-based photometers exhibit reduced social interactions (14 s compared to ~21 s), total activity (~75 m compared to ~100 m) and compromised mobility (~6 cm/s compared to ~9 cm/s), with less time spent in the center of the experimental enclosure (~30 s compared to ~70 s), consistent with increased levels of anxiety.<sup>60</sup> These and other results suggest that wireless systems can significantly improve the validity of animal studies by minimizing the effects on motion. The wireless system used in this study also reduces the requirements for supporting equipment and interface hardware, thereby decreasing the overall cost of the system to less than \$100, much lower than the typical cost of a fiber-based photometry system (~\$20,000).<sup>60</sup> Similar considerations in costs and constraints apply for recording and modulation schemes based on electrical and fluidic approaches.<sup>61, 62</sup> Electrophysiological recordings from cortices of bats during social engagements indicate the development of correlated neural activities across the multiple brains.<sup>63</sup> Vocalization-correlated neural signals occur frequently and in manifold forms in unrestrained animals in social groups.<sup>64</sup> From a biomedical standpoint, studies of unrestrained animals reveal neuromodulatory therapeutic outcomes that are difficult to observe from restrained test subjects. For example, stimulating neurons in the Right Crus of an autism mouse model can rescue social impairments, revealing the therapeutic potential of cerebellar neuromodulation in autism spectrum disorders.<sup>65</sup>

Current tethered systems pose particularly significant problems for use with non-human primates and other animal models that are more dexterous and possess greater physical strength than rodents.<sup>64</sup> Emerging interest in neuroscience research towards the characterization of generalizable aspects of the central and peripheral nervous system has shifted the focus of researchers to the study of animal models other than rodents. The use of tethered systems, however, in species of fish,<sup>66, 67</sup> bats,<sup>68</sup> birds,<sup>69</sup> monkeys<sup>64</sup> and others (Figure 1d), is particularly challenging and limits the animal subject diversity. Although devices with implantable microscale recording and stimulating probes can be made fully wireless with head stages that house battery packs and electronics<sup>59, 70-72</sup> the use of percutaneous connections expose the animals to high risks of infection and require frequent human interactions to recharge or replace the batteries.

## Design considerations for fully implantable devices.

Mechanical and biochemical forms of mismatch at the biotic-abiotic interfaces can cause insertion-related trauma and resulting chronic inflammation reaction in the host neural tissues<sup>73, 74</sup>. In many cases, these foreign-body responses can degrade the sensitivity and stimulation efficiency of the measurements<sup>75, 76</sup>. Engineering approaches to minimize these effects demand combined attention to mechanics,<sup>77</sup> materials<sup>73</sup> and physical form factors.<sup>78</sup> In particular, the mechanical characteristics of implants, including those of biointerfaces, interconnects, control circuits, power harvesting modules and communication units, play crucial roles in the onset of foreign-body reactions<sup>79</sup> as devices with high stiffnesses tend to induce large insertion-related lesions<sup>16, 60, 80</sup> as well as increased inflammation reactions and neuronal apoptosis due to their motion, relative to soft tissues.<sup>57, 58</sup> Eliminating the mechanical mismatch between soft biological materials and implantable devices enables not only soft neural interfaces but also devices with system-level mechanical compliance,

thus allowing for minimally disruptive integration and intimate interfaces with the central and peripheral nervous systems at anatomically complex and dynamic locations.<sup>3, 73, 81, 82</sup> Devices with stiffnesses close to those of tissues can be realized by using mechanically compliant materials<sup>83</sup> or hybrid structures of stiff materials and soft supports<sup>84</sup>, such as conjugated polymers<sup>85, 86</sup> and carbon nanomaterials<sup>87, 88</sup>, buckled nanoribbons<sup>89</sup>, serpentine nanowires,<sup>90</sup> as well as mesh structures<sup>91</sup> of metals and semiconductors. Substrate materials often determine the effective mechanical properties of the devices, and both approaches rely on flexible or stretchable substrates, most typically polyimide<sup>86</sup> or Parylene<sup>92</sup> for the former and polydimethylsiloxane (PDMS)<sup>77</sup> for the latter. Conformal surface mounting sheets<sup>93-97</sup> or soft penetrating probes<sup>60, 98-100</sup> can be used to build soft neural interfaces capable of interacting with the skin or other organs for recording physiological signals and delivering neural stimuli.<sup>1, 3</sup>

Wireless and fully-implantable systems also require mechanically compliant electronic components for control, power harvesting and data communication.<sup>95, 96, 98, 100-102</sup> Serpentine metal traces with shapes that ensure high conductivity ( $\sim 4 \times 10^5$  S/cm) under tensile strains of up to 300%,<sup>103</sup> can be used for structured antennas and interconnects that provide reliable operation for strains that exceed those set by natural biological motions, i.e. less than 20-50%.<sup>98, 104, 105</sup> In systems that demand active electronics, off-the-shelf components such as microcontrollers and radio units are attractive because of their commercial availability and low cost, capable of assembly on flexible/stretchable substrates with serpentine interconnects<sup>96</sup> and strain-isolating mechanical designs<sup>95</sup> to support requirements in deformability.<sup>95, 96, 102</sup>

With the exception of temporary implants based on bio-resorbable materials,<sup>106</sup> most devices require barriers to biofluids as a means to avoid electrical shorting and ionic contamination of the functional elements during extended operational periods in corrosive biologic fluids.<sup>107</sup> Material choices for such barriers must meet requirements in biocompatibility and low water and ion permeability.<sup>108</sup> Optogenetic stimulators encapsulated by biocompatible bilayers of parylene/PDMS<sup>109</sup>, for example, can operate during immersion in physiological saline solution at 60 °C for at least 90 days, corresponding to projected lifetimes of up to a year at 37 °C,<sup>100</sup> maintain mechanical flexibility and proper functionality.<sup>102</sup> Compared to polymers, inorganic materials such as ceramics and metals offer enhanced levels of hermeticity.<sup>110</sup> Physically transferred layers of silicon dioxide (thicknesses of  $\sim 1$   $\mu$ m) grown thermally on silicon wafers provide projected stability as biofluid barriers for timescales of many decades ( $>70$  years) in simulated physiological conditions.<sup>111</sup> Additional capping layers (i.e. hafnium dioxide) can further enhance the long term stability by reducing the transport of ions and by slowing the rates of hydrolysis. Additional details on biofluid barriers for chronically stable bioelectronic systems appear elsewhere.<sup>112</sup>

## Power sources and wireless communication.

Conventional small and lightweight batteries can satisfy the power requirements for wireless devices with sophisticated function, as demonstrated in optoelectronic photometers for monitoring neuronal dynamics in the deep brain,<sup>60</sup> and in optofluidic systems for

programmable pharmacology and optogenetics.<sup>16</sup> Batteries with sufficient storage capacity however, have sizes ( $> 3 \text{ cm}^3$ ) and weights ( $> 2\text{g}$ )<sup>71</sup> that require percutaneous wiring in small animals<sup>113</sup>, and recharging disrupts the continuity of experiments.<sup>114</sup> Batteries often occupy up to 90% of the volume<sup>115</sup> and account for more than 60% of the weight<sup>60</sup> of implantable devices; their downscaling, or ideally their complete elimination, would provide significant advantages, especially for devices fabricated on polymeric substrates and in ultra-thin form factors<sup>98, 102</sup>.

Wireless power delivery schemes provide attractive alternatives, and offer lightweight, miniaturized form factors with indefinite operational lifetimes<sup>116, 117</sup> (Figure 2a) that rely on body-generated power, (such as kinetic energy harvested from skeletal<sup>118</sup> and visceral motions,<sup>119</sup> chemical energy from blood sugar<sup>120</sup> and/or thermal energy from body heat<sup>121</sup>) or external power transmitted via radio frequency (RF) radiation,<sup>100, 101, 122</sup> light illumination<sup>123, 124</sup> or ultrasonic vibrations<sup>125, 126</sup> (Table 1). Power supplies must be tailored for specific applications due to variable system-dependent power consumption requirements. For example, electrophysiological recording based on optimized application-specific-integrated-circuits (ASICs) can consume as low as a few  $\mu\text{W}$  per channel<sup>34, 127-130</sup>, while photometric recording typically requires average powers in the range of  $\sim \text{mW}$ <sup>131</sup>, yet even with the same operation modality, power consumption may differ between implant locations<sup>100, 119, 122, 132</sup> (Table 2).

### Internal power harvesting

Power derived from internal biological sources, including mechanical<sup>119, 133, 134</sup>, biochemical<sup>135, 136</sup>, bioelectrical<sup>137, 138</sup>, and thermal forms of energy<sup>139</sup>, have the potential to enable self-contained, fully autonomous operation<sup>116, 140</sup>. The relatively low output power available from these sources, however, limit applications to narrow classes systems that do not require advanced control electronics or radios, such as simple interfaces for cardiac pacing and pulsatile neurostimulation<sup>119, 134</sup>. Additionally, the intermittency and physiological load associated with power derived from biological processes may affect the reliable operation of the implants and the health of the host organism. By contrast, and as explained in subsequent sections, external power sources, including those that rely on RF radiation<sup>98, 122</sup>, magnetic coupling<sup>100, 141</sup>, optical illumination<sup>124, 142</sup> and ultrasonic waves<sup>125, 126</sup>, decouple the device operation from the biology, with capacity for providing reliable, constant power supply for multimodal physiological recording<sup>131, 143</sup>, optofluidic neuromodulation<sup>62, 144</sup> and closed-loop regulation of organ functions<sup>141</sup>. Depending on the harvesting mode, externally powered systems fall into two categories. The first involves far-field RF radiation<sup>98</sup> or near-field magnetic coupling<sup>100</sup>, where the wireless power link connects to transmitters installed on or around the animal's cage<sup>145</sup>. The RF waves or magnetic fields hence fill the entire test space or may selectively couple to an animal<sup>122</sup>, independent of its location<sup>102</sup>. The second category includes imaging setups for optical illumination<sup>123</sup>, direct body contacts for ultrasound<sup>126</sup>, and proximity antennas for weak inductive coupling between transmitting and receiving coil<sup>146</sup>. Although these schemes can be realized in devices with sub-millimeter dimensions<sup>123, 124, 146</sup>, they cannot be easily configured to operate across an entire test space, thereby leading to significant constraints on experiments in freely moving animals<sup>123, 124, 146</sup>.



Piezo and triboelectric effects allow conversion of the kinetic energy of voluntary (skeletal) and autonomic (cardiovascular, respiratory and gastrointestinal) muscular motions into electrical energy,<sup>117, 119, 133, 134, 147</sup> with the potential to allow for autonomous device operation, without separate power supplies.<sup>140</sup> A flexible triboelectric nanogenerator (TENG) for weight control generates biphasic pulses of electrical current in response to peristalsis of the stomach<sup>119</sup>, stimulating the vagal afferent fibers to reduce food intake (figure 2b). Other work demonstrates that bending of a flexible  $\text{Pb}(\text{In}_{0.5}\text{Nb}_{0.5})\text{O}_3$ – $\text{Pb}(\text{Mg}_{0.33}\text{Nb}_{0.67})\text{O}_3$ – $\text{PbTiO}_3$  (PIMNT) piezoelectric device can create pulsed electric current for stimulating the motor cortex of mice (Figure 2c), as a self-powered device for deep brain stimulation (DBS).<sup>118</sup> The extracorporeal piezoelectric generator connects to the stimulation probe via copper wires and a linear stage creates the necessary cyclic bending deformations. Control electronics with sufficient energy efficiency and continuous, predictable harvesting capabilities will be needed to construct fully implantable systems. The primary disadvantages of all electromechanical energy scavenging technologies are the limited amount of available power and its pulsatile, often intermittent, nature.<sup>116</sup> Most devices that depend on skeletal motion generate a peak powers of less than 1 mW with low duty cycles, and considerable reductions after rectification.<sup>118</sup> Power levels in the range of tens of  $\mu\text{W}$  (power density of  $\sim 11 \mu\text{W}/\text{cm}^2$ ) can be expected from visceral motions,<sup>119, 133</sup> which, even in conjunction with capacitors or other components for energy storage, is typically insufficient for microcontrollers,<sup>102</sup> optoelectronic devices,<sup>60</sup> microfluidic actuators,<sup>16</sup> or wireless communication systems. As a result, existing piezo/triboelectric generators are relevant for passive devices with simple functions, such as the production of pulsed voltages for pacemakers and instantaneous neural stimulation, requiring peak powers of tens of  $\mu\text{W}$ .<sup>133, 134, 148</sup>

Other forms of energy scavenging include bio-fuel cells<sup>120, 136, 149, 150</sup> and thermoelectric generators.<sup>121, 133</sup> Such systems are of interest because the corresponding energy sources such as glucose, oxygen or thermal gradients are always present in living organisms, however they have modest power outputs. For instance, normal temperature gradients between the skin and ambient air ( $\sim 10 \text{ K}$ )<sup>121</sup> provide a thermoelectric power of only  $\sim 28.5 \mu\text{W}/\text{cm}^2$ . The expected output power of bio-fuel cells falls in a similar range, i.e.  $\sim 10 \mu\text{W}/\text{cm}^2$ .<sup>135, 151</sup> Nevertheless, research efforts on implantable bio-fuel cells in a range of host organisms such as insects,<sup>152</sup> snails,<sup>153</sup> rats<sup>154</sup> and rabbits<sup>149</sup> shows some promise. A recent study demonstrates wireless operation of enzymatic bio-fuel cells implanted in freely behaving rabbits where battery-powered Bluetooth-based modules control and monitor the bio-fuel cell performance (Table 1).<sup>149</sup> These systems yield powers of  $\sim 1.6 \mu\text{W}/\text{cm}^2$  (estimated from a biocathode and bioanode thickness of  $\sim 1 \text{ mm}$ ) for 30 min each day, over 16 consecutive days, followed by reductions over 60 days of implantation. Device degradation follows mainly from inflammatory reactions, biofouling and degradation of the biocatalysts,<sup>135, 155</sup> whereas the effects of continuous harvesting on the target organism require further investigation.<sup>155</sup>

### Radio-frequency power transfer

Dedicated power delivery schemes based on transmission via electromagnetic (EM) radiation, acoustic vibrations or other means are often attractive, as they outperform the

scavenging schemes described above in the amount and stability of the output power.<sup>116, 140</sup> Here, significant amounts of power (up to  $\sim 500$  mW)<sup>156</sup> can be transmitted reliably, with versatile design and deployment options. The three main categories of remote power harvesting technologies include far-field RF transmission, near-field magnetic resonant coupling, and ultrasound transduction. In the first approach, RF radiation (frequency of 420 MHz  $\sim$  2.4 GHz, wavelength of 0.1 – 1 m) emitted by a transmission antenna is captured by a harvesting antenna and converted by a rectification circuit into DC power to drive the electronics.<sup>157</sup> Transmission can occur over long distances (up to meters or more) and, with specialized primary antenna designs, uniform and continuous power delivery can be achieved throughout typical experimental arenas ( $\sim 30$  cm by 30 cm).<sup>98</sup> Concepts in stretchable electronics<sup>96</sup> can be leveraged in this context to create mechanically soft antennas and rectifying circuits in fully-implantable miniaturized optoelectronic systems for optogenetic modulation of the spinal cord and the peripheral nerves (Figure 2d).<sup>98</sup> Here, the antennas (size of  $\sim 3$  mm  $\times$  3 mm) harvest RF power through capacitive coupling between adjacent serpentine traces, to enable compact, lightweight devices (overall size of  $\sim 0.7$  mm  $\times$  3.8 mm  $\times$  6 mm, overall weight of  $\sim 16$  mg) with low-modulus system-level mechanics (effective modulus of  $\sim 1.7$  MPa), capable of accommodating irregular anatomic shapes and natural motions. Advanced antenna designs allow for multimodal operation, where spatially separated  $\mu$ -ILEDs with multiple emission wavelengths (540 nm and 465 nm) can be independently powered by multiple antennas that resonate at distinct frequencies.<sup>101</sup> Active, motion-tracking primary antenna arrays can enable localized power delivery by improving the harvesting efficiency. Given an input RF power of 2 W across a cage of 25 cm by 25 cm,  $\mu$ -ILEDs for optogenetic stimulation can be activated while the animal subject is freely moving with an irradiance of 10 mW/mm<sup>2</sup>, corresponding to a power density of  $\sim 1.42 - 2.88$  mW/cm<sup>2</sup>.<sup>98, 101</sup> A disadvantage of far-field transmission is the strong dependence of the efficiency on the angle between the transmission and receiving antennas. This dependence follows from the tradeoff between angular acceptance and antenna gain, where high gain is often required to cast sufficient power.<sup>158</sup> As a result, considerable efforts in antenna design<sup>159</sup> and transmitter deployment strategy<sup>101</sup> are required to achieve reliable power harvesting. Additionally, RF transmission, especially at higher frequencies (1-4 GHz), can be affected by interference caused by environmental obstructions. In particular, conductive objects such as metals can nearly completely reflect RF waves in the relevant frequency range (0.5 – 4 GHz), and dielectric materials with high refractive index also reflect the RF waves significantly.<sup>160</sup> The interference between the incoming RF wave and reflected/scattered wave results in spatially varying RF power density in the test space<sup>160</sup>, and, in extreme cases, the formation of hotspots and dead zones, leading to potentially high specific absorption rates (SARs) and lack of power supply, respectively. One strategy to overcome these issues exploits an RF cavity that resonantly excites electromagnetic fields that are spatially confined in the body of the animal, thus enabling self-tracking operation albeit with relatively high SAR levels, up to  $\sim 6.2$  W/kg.<sup>122, 161</sup> This high SAR value follows from the strong absorption by moisture and biological tissues at these RF frequencies, leading in some cases to levels of heating that can alter essential biological activities.<sup>162</sup> High tissue absorption at elevated frequencies is especially a concern for power harvesting efficiency of fully-implanted devices. This effect limits the amount of power that can be delivered without adverse biological impact.



## Near-field wireless power transfer

First demonstrated by Nikola Tesla,<sup>163, 164</sup> near-field power transfer exploits nonradiative electromagnetic energy (within  $\sim \lambda/2\pi$  from the transmitter) and relies on inductive coupling between a transmitting coil and a receiving coil.<sup>165</sup> Such schemes offer efficient means for wireless power transmission over short distances, with commercial applications for charging electric vehicles<sup>166, 167</sup> and consumer electronics.<sup>168</sup> Nonetheless, shortcomings such as high sensitivity to axial and angular alignment between coils as well as limited transfer range (less than a few centimeters) create challenges in the applications to implantable devices.<sup>165</sup> The power transfer efficiency and distance can be significantly improved by adopting transmitting and receiving resonators that are tuned to create strong magnetic resonant coupling.<sup>169, 170</sup> Efficient power transfer can be achieved with high quality factor (Q-factor) resonators over large distances of up to a few meters<sup>169</sup> where the power transfer efficiency is negligible, without resonant coupling.<sup>170</sup> Because of its non-radiative nature, magnetic resonant coupling (with frequencies ranging from  $\sim 100$  kHz<sup>171, 172</sup> to  $\sim 200$  MHz<sup>173</sup>) is less sensitive to changes in dielectric environments and to the presence of conductive obstacles, as demonstrated by the successful power transfer in cases where the line of sight between the two resonators are completely obstructed,<sup>169</sup> resulting in the elimination of dead-zones and hotspots. Low frequencies in this range benefit from reduced tissue absorption,<sup>162</sup> and thus larger penetration depth and minimized adverse biological effects, albeit with the requirement for large receiving coils. High frequencies improve the device efficiency<sup>169</sup> and reduce its size.<sup>174</sup> In practical applications, 13.56 MHz (wavelength  $\sim 12$  m) is attractive because its absorption lies in an acceptable range (Table 1)<sup>175</sup> and the frequency aligns with radio-frequency identification (RFID) and emerging near-field communication (NFC) standards.<sup>104</sup> In addition, communication can be implemented along with power transfer at the same carrier frequency to allow for wireless control and data transmission using NFC protocols.<sup>176, 177</sup> Magnetic resonant coupling at 13.56 MHz for advanced classes of wearable and implantable electronics<sup>178, 179</sup> occurs between two resonant systems, a primary coil enclosing a test arena, and a secondary coil powering the implant.<sup>100, 102, 104, 143</sup> In these experimental setups, the power transfer efficiency depends weakly on orientation or location of the secondary coils.<sup>180</sup> Consequently, reliable power harvesting (up to 12 mW<sup>143</sup> for small rodent sized devices) with  $\sim 13$  mW/cm<sup>2</sup> can be achieved throughout a desired cage volume (determined by the size of the primary coil and the RF power source) and complex test environments can be addressed with simple antenna designs or deployment strategies.<sup>102</sup> With on-board circuits and electronic components encircled by the secondary coil, devices with miniaturized form factors (diameter  $\sim 5$  mm, weight  $\sim 16$  mg) are possible, in encapsulated constructs that are biocompatible and chronically stable.<sup>102</sup> Magnetic resonant coupling depends on magnetic flux captured by the secondary coil, with minimal sensitivity to its detailed shape. As a result, the overall device geometry can be easily adapted to accommodate various anatomical structures and the dynamic nature of biological tissues. In addition, fabrication techniques compatible with well-established flexible printed circuit board (PCB) technologies and with off-the-shelf components ensure standardized and scalable manufacturing, facilitating the potential for broad dissemination.<sup>102</sup> A further advantage of magnetic resonant coupling is its low SAR<sup>175</sup> that follows from the approximate power law relationship of this quantity with relatively low frequencies

(~ 100s kHz – 10s MHz)<sup>165</sup> used in magnetic resonant coupling, thereby minimizing safety concerns during long-term operation. These advantages allow implementation in a wide range of wireless, battery-free and fully implantable devices capable of localized tissue oximetry,<sup>143</sup> bioresorbable monitoring of intracranial pressure and temperature,<sup>106</sup> optogenetic stimulation for the central and peripheral nervous systems and pharmacological modulation.<sup>100, 144</sup> A subdermally implantable device powered by magnetic resonant coupling allows for optogenetic stimulation of regions of the deep brain, with reliable operation and good chronic stability via an ultrathin, injectable probe with a  $\mu$ -ILED at its tip<sup>123</sup> (Figure 2e). The small footprint (diameter ~ 9.8 mm, thickness < 1.3 mm after encapsulation) and lightweight construction (~ 30 mg) of the device, along with its mechanical flexibility, allow for stable output power when bending to radii of curvature < 5 mm. A double-loop primary coil allows simultaneous operation of a large collection of devices in all regions of a standard home cage (30 cm  $\times$  30 cm) with good spatial uniformity (variation of light intensity on the same height is less than 30%). A bi-layer encapsulation of parylene and PDMS, as described previously, ensures good bio-compatibility and long-term stability. The devices can operate continuously in complex environments that contain obstructions and metal surroundings, including water tanks. The power transfer efficiency (PTE) of magnetic resonant coupling is determined by the coupling coefficient ( $\kappa$ ) between the primary and secondary coils, as well as their quality factors (Q-factor)<sup>165</sup>. Both  $\kappa$  and Q-factor decrease with the coil size, leading to reduced PTE for devices with footprints < 10 mm<sup>2</sup> and  $\kappa$  decreases rapidly with the distance (and lateral misalignment) between primary and secondary coils<sup>165, 181</sup>. Ultraminiaturized implants<sup>146</sup> therefore require optimized magnetic coupling schemes and coil designs, yet can be mitigated, for small animals, by employing primary coils that enclose the test arena<sup>100</sup>. Similar schemes for large animal experiments are less practical, as high levels of input power are needed to maintain useful magnetic energy densities across areas of interest. An additional consideration is in reducing the resistance of the conductive traces to achieve coils with high Q-factors. Optimization requires a balance between trace thicknesses, overall dimensions and mechanical bending stiffnesses<sup>98, 102</sup>. Despite these challenges, near-field magnetic resonant coupling represents the most widely adopted technology for operating wireless, battery-free implants for small animals, with options in various advanced functions in physiological recordings,<sup>143</sup> optogenetic stimulation,<sup>102</sup> and pharmacological modulation.<sup>176</sup>

### Photonic Power transfer

EM radiation from visible and near-infrared light can also be exploited for power delivery.<sup>123, 124, 142, 158</sup> For example, dual-junction gallium arsenide (GaAs) solar cells with conversion efficiencies of 25% are sufficient to operate control logic circuits and injectable  $\mu$ -ILEDs for optogenetic stimulation. Compared with systems powered only by RF radiation, addition of these solar cells, for a 1-sun light source, can reduce the amount of required RF power by at least ten-fold.<sup>158</sup> Microscale GaAs solar cell (3  $\times$  5  $\mu$ -SC) arrays, built on multi-layer GaAs wafers by standard microfabrication techniques and transfer-printed onto flexible substrates, can operate blue and yellow  $\mu$ -ILEDs at intensities of 3.5 and 2.3 mW/mm<sup>2</sup> (~ 19 mW/cm<sup>2</sup> with array area of 6 mm  $\times$  2 mm) under IR illumination (774 nm; with an intensity of 200 mW/cm<sup>2</sup>) and can also power wireless optogenetic devices.<sup>142</sup> Recent developments in the monolithic integration of

microscale optoelectronic devices serve as a practical basis for power harvesting in ultra-miniaturized wireless implants<sup>123, 124</sup>. For example, a thin-film, up-conversion device that combines an IR double junction photodetector (DJPD) and a visible LED, both based on III-V semiconductor optoelectronic technologies<sup>124</sup> captures photons (810 nm) from an external source and generates photovoltaic (PV, power density  $\sim 2.1 - 9.5 \text{ mW/cm}^2$ ) current that, in turn, powers the LED to realize visible light (590 – 630 nm) emission for optogenetic stimulation (Figure 2g). A miniaturized, wireless optoelectronic neural interface (microscale optoelectronically transduced electrodes, MOTEs) integrates 180-nm complementary metal-oxide-semiconductor (CMOS) circuits to amplify and encode neural signals, with an AlGaAs photodiode that switches between PV, for power harvesting (with power density of  $\sim 12 \text{ mW/cm}^2$  on a diode area of  $\sim 50 \mu\text{m} \times 80 \mu\text{m}$ ) and LED modes for data communication (near-IR emission) with external systems.<sup>123</sup> By eliminating the need for RF antennas or ultrasonic transducers, this ASIC device enables small implants ( $4.7 \times 10^{-3} \text{ mm}^3$ ) with low power consumption (1  $\mu\text{W}$ ), as the potential foundations for high spatial resolution electrophysiological recording/stimulation at specific discrete sites within single neurons or single muscle fibers.

An analysis of total power requirements for these approaches, assuming uniform illumination of an experimental arena, is instructive. For example, in the case of the DJPD up-conversion device, the IR intensity required to generate useful optical emission is  $15 \text{ mW/mm}^2$ , which corresponds to a power of 562.5 W for a home cage ( $15 \text{ cm} \times 25 \text{ cm}$ ).<sup>124</sup> Similarly an IR intensity of  $200 \text{ mW/cm}^2$  for the GaAs  $\mu\text{-SC}$  array corresponds to a total power of 75 W.<sup>142</sup> The green light used to power the MOTEs is  $100 \text{ mW/mm}^2$ , equivalent to 3750 W.<sup>123</sup> Further assuming IR LED efficiencies  $\sim 40\%$  and considering power losses due to absorption/scattering by the scalp, skull and brain tissues,<sup>182</sup> leads to power levels that are high for practical use. Optical imaging/tracking systems and/or focusing optics will be required for such technologies, some of which may restrict the operational environments with freely behaving animals. The output power of solar cells depends strongly on incident angles<sup>183</sup>, which may further limit device operation when the animals rotate and twist.

### Ultrasonic power transfer.

Ultrasound waves emitted by a transducer travel inside the body to the location of a device where they are converted to electrical power by a piezoelectric crystal.<sup>140, 184, 185</sup> Such waves propagate with a velocity  $10^5$  times slower – thus have much shorter wavelengths (0.3 - 0.7 mm for ultrasound used in medical imaging) at similar frequencies – than EM waves. As a result, focused power delivery may be achieved with high spatial resolution for implantable medical devices.<sup>186</sup> For example, a miniaturized, implantable ultrasonic backscattering sensor composed of a piezocrystal, a transistor and a pair of electrodes allows wireless recording of electromyogram (EMG) and electroneurogram (ENG) data (Figure 2f)<sup>126</sup>. A disadvantage of this communication scheme is that ultrasonic waves propagate directionally. As a result, slight misalignments and misorientations between the external transducer and implanted receiver lead to reductions in coupling efficiency and increases in signal noise. Additionally, the transducer must contact the skin to eliminate a large impedance mismatch at the tissue-air interface. The large size of commercially available transducers hinders the practical implementation of this approach in awake and

freely behaving small animals. One possible solution to these challenges exploits beam steering strategies enabled by miniaturized and wearable transducer arrays operated using sophisticated control algorithms.<sup>187</sup> Another challenge is that high performance, inorganic piezoelectric crystals have brittle mechanical properties, comparatively high mass densities and rigid, planar characteristics that limit their applications in small animals for which high power output and mechanical compliance are essential. For example, assuming a typical acoustic-to-electrical conversion efficiency of 2%<sup>181</sup> (maximum efficiency ~25% for perfect alignment between the transducer and receiver<sup>126</sup>) and an implant cross-section of ~1 mm<sup>2</sup>, generating ~1 mW at the implant, requires an ultrasound intensity of 50 mW/mm<sup>2</sup>, nearly one order of magnitude higher than the FDA approved limit in ultrasonic exposure (7.2 mW/mm<sup>2</sup>).<sup>188</sup> To generate sufficient power (> 10 mW) for applications such as optogenetics with ultrasonic power densities within the safety limit, the piezocrystal must present an area of at least 1 cm<sup>2</sup>, leading to a weight of, in the case of PZT, at least ~760 mg for the piezocrystal alone. Furthermore, with a standard transducer output intensity of 0.4 mW/cm<sup>2</sup>, the required area of the transducer (~125 cm<sup>2</sup>) and the battery storage capacities for this scenario may pose practical difficulties for small animal models.

The fundamental limit for ultrasonic power delivery is set by the local rate of heat generation (Q) that follows from the absorption of ultrasound waves, as defined by  $Q = 2\alpha f I_{SPTA}$ , where  $\alpha$  (dBcm<sup>-1</sup>MHz<sup>-1</sup>) is the attenuation coefficient,  $f$  (MHz) the ultrasonic frequency and  $I_{SPTA}$  (mW/cm<sup>2</sup>) the de-rated spatial peak time average intensity.<sup>189</sup> Values of  $\alpha$  for soft tissue, bone tissue and lung are ~0.4, ~20 and ~40, respectively.<sup>190</sup> Therefore, the local rates of heat generation calculated using reported ultrasonic frequencies and intensities<sup>125, 126, 186</sup> are ~0.3-240 mW/cm<sup>3</sup>, ~8-6000 mW/cm<sup>3</sup> and ~15-12000 mW/cm<sup>3</sup> for soft tissues, bones and lung, respectively (Table 1). The relatively moderate absorption of ultrasound by soft tissues potentially enables large penetration depths,<sup>181</sup> but the presence of highly absorbing bone may induce significant heating effects<sup>191</sup> and low ultrasonic frequencies may induce cavitation.<sup>189</sup>

Overall, recent successful efforts to minimize size and mechanical loads associated with conventional electrochemical power sources utilizing wireless, lightweight systems that support advanced neuromodulation and sensing capabilities for the use in small animals. This new generation of tools enables the dissection of the peripheral and central nervous systems in freely moving animal models and forms the technological basis for the translation to large animal models, non-human primates and human applications.

## Operation modes.

Operation modes can be tailored via power delivery schemes and device configurations for different anatomic locations, recording and modulation settings. For instance, implantation in the brains of mice is only possible with small (< 1 cm<sup>2</sup>), lightweight (< 0.5 g) devices. Simple stimulation can be realized by passive components, where changes in the frequency and duty-cycle of the power transmitter control the temporal pattern and strength of stimulation. Examples include devices powered by RF transmission<sup>98, 122</sup> or magnetic coupling<sup>193</sup>, for stimulation of the deep brain<sup>100, 122</sup>, spinal cord<sup>122, 193</sup> and peripheral nerves<sup>98, 122</sup>. Systems with independently addressable bio-interfaces stimulating distinct

anatomical locations at the cellular<sup>194</sup> and circuit level<sup>195</sup> require multichannel wireless operations that can be addressed by passive multiresonance antennas. Active components can support the digital control of individual and multiple devices<sup>102</sup>, eliminating issues of spatial- and orientation-dependent RF coupling. Pre-defined program states stored in the non-volatile memories of low-power microcontrollers control the magnitude and spatial/temporal patterns of multiple stimulators in individual or multiple devices<sup>102</sup>. Monolithic integration of multifunctional neuromodulation devices feature a combination of soft microfluidic channels and  $\mu$ -ILED probes for programmable and coordinated delivery of pharmacological and optogenetic stimuli, configured as injectable probes for insertion into regions of the deep brain<sup>62</sup> and as soft cuffs for wrapping peripheral nerves<sup>144</sup>.

For wireless, fully-implantable devices that involve physiological recording capabilities, uplink communication systems send data to external receivers for storage and further processing<sup>196</sup>. Solutions using protocols based on Bluetooth radios, near-field communication (NFC), ultra-wideband (UWB), infrared communication (IR) and ultrasonic backscattering, each have distinctive advantages and disadvantages in terms of data rate, operation distance and inherent compromise in form factors and power consumption<sup>197</sup>.

Infrared LEDs for optical communication provide viable options, with footprints  $< 1 \text{ mm} \times 0.5 \text{ mm}$  and power consumptions  $< 0.5 \text{ mW}$ <sup>131</sup>, for data rates at  $\sim 27 \text{ Hz}$  with 12-bit resolution, sufficient for capturing temporal variations in rStO<sub>2</sub> (regional oxygen saturation level) associated with tissue perfusion and global O<sub>2</sub> levels (below 1 Hz)<sup>143</sup> as well as neuronal calcium dynamics<sup>60, 131</sup>. An optical uplink can also be used for both power supply and data transmission in ASIC-enabled electrophysiological recording devices with sub-millimeter form factors and with potential for fully-implantable operation<sup>123</sup>.

Systems that integrate neural recording with neuromodulation in an open-loop or closed-loop fashion have additional requirements for bidirectional communication<sup>61, 107, 145, 196, 198</sup>, such as downlinked control commands and uplinked recorded signals via the same or a separate mechanism.<sup>196</sup> Closed-loop feedback involves real-time adjustment of the timing and amplitude of modulation (stimulation or inhibition) in response to neural activity or physiological responses, and is clearly advantageous over open-loop systems, particularly for therapeutic purposes<sup>107, 199</sup>. Significant engineering challenges are faced by retaining the key features needed for operation in this mode and in an implantable platform compatible for unconstrained animal experiments. An example of wireless, closed-loop system, capable of regulating bladder function in a rat, combines magnetic resonant coupling with Bluetooth Low Energy (BLE) protocols for power supply and bidirectional data transmission, respectively<sup>141</sup>, and records biophysical signals related to bladder filling and voiding via BLE to an external device, and automatically identifies bladder dysfunction and transmits control commands to activate  $\mu$ -ILEDs for optogenetic regulation of voiding events.

ASICs designed for implantable wireless physiological recording and neuromodulation can vastly improve the characteristics of systems that rely on discrete off-the-shelf components, by facilitating ultra-low power requirements (down to the nW level<sup>129</sup>), exceptionally small form factors (down to the sub-mm level<sup>123, 146</sup>), and high integration densities ( $>100$

channels<sup>61, 200</sup>). The performance gains in ASICs follow from specialized circuit designs that omit flexible and programmable control structures however, limits their versatility. Also, each application requires a cycle of design, development and production, in a lengthy and costly process that delays further refinement and modification. As a result, ASICs have limited appeal for exploratory research by individual investigators or small university teams, where requirements and functionalities are often not clearly defined. As a result, in spite of numerous impressive research demonstrations, only a few ASICs (e.g. Intan microsystem chips for multiplexed recording and stimulation and Neuropixel probes of the deep brain with integrated amplification) have been deployed and adopted for neuroscience research. By contrast, off-the-shelf components offer significantly more flexibility and cost-effectiveness, rapid implant design and verification, in a scalable format.

### Optogenetic stimulation.

Microscale optoelectronic components enable highly miniaturized devices for *in vivo* optogenetics, such as  $\mu$ -ILEDs with lateral sizes of  $10 \times 15 \mu\text{m}^2$ , and thicknesses of  $0.5 \mu\text{m}$ ,<sup>53</sup> with a wide range of options in emission wavelengths (i.e., UV, blue, green, yellow, and red) and optical output intensities ( $50 \text{ mW}/\text{mm}^2$  and more<sup>53, 100</sup>), suitable for most optogenetic experiments (i.e.  $1\text{-}21 \text{ mW}/\text{mm}^2$  ChR2,<sup>45, 98, 122, 201-203</sup> C1V1,<sup>203</sup> ReaCHR,<sup>204</sup> and NpHR<sup>203, 205</sup>). In pulsed mode operation, the maximum steady state temperatures at the interface with the tissue are less than at most a few tenths of a degree Celsius<sup>102</sup>, well below the safety thresholds ( $2\text{-}5 \text{ }^\circ\text{C}$ ) for irreversible tissue damage<sup>206, 207</sup>, and the  $2 \text{ }^\circ\text{C}$  limit for neuro stimulators,<sup>208</sup> and the approximate  $1 \text{ }^\circ\text{C}$  for thermal neuromodulation<sup>209</sup>, set by the American Association of Medical Instruments. Such  $\mu$ -ILEDs have electrical operating requirements that can be satisfied with the classes of wireless power sources described in the previous section. For example, fundamental studies indicate levels of irradiation suitable to stimulate single neuronal units ( $0.1\text{-}0.2 \text{ mW}/\text{mm}^2$ ) and to activate groups of ChR2 expressing neurons ( $1 \text{ mW}/\text{mm}^2$ ) at the surface ( $150 \mu\text{m}^2$ ) of an InGaN  $\mu$ -ILED operated with  $\sim 10 \mu\text{W}$  ( $\sim 2.9\text{V}$  and  $\sim 3 \mu\text{A}$ ) and  $\sim 25 \mu\text{W}$  ( $\sim 3.1 \text{V}$  and  $\sim 8 \mu\text{A}$ ) of electrical power, respectively.<sup>53</sup> Additional optical power can yield volumetric illumination to evoke strong behavioral effects. The typical electrical power associated with  $\mu$ -ILEDs for optogenetic stimulation in freely behaving animals is  $1\text{-}3 \text{ mW}$ , to yield light intensity of  $\sim 10 \text{ mW}/\text{mm}^2$ ,<sup>98-100</sup> which remains within a range accessible to wireless schemes discussed previously.

Representative, miniaturized optogenetic platforms interfaced to these  $\mu$ -ILEDs use different schemes of wireless controls and power supplies based on lightweight ( $\sim 700 \text{ mg}$ ) power harvesters (910 MHz, far-field RF transmission, panel antenna) with sets of gallium nitride  $\mu$ -ILEDs ( $50 \times 50 \times 6.5 \mu\text{m}^3$ ) on thin ( $6 \mu\text{m}$  thick) polyester probes<sup>99</sup> (Figure 3a). This design architecture also enables multimodal operation via the combined integration of  $\mu$ -ILEDs, photodetectors, temperature sensors and platinum electrodes for simultaneous optogenetic stimulation, thermal monitoring, and electrophysiological recording at the same location in a targeted area of the deep brain. Mechanical compliance and flexibility of the probe (total thickness of  $20 \mu\text{m}$  and width of  $300 \mu\text{m}$ ) reduces glial activation and lesion sizes compared to those of optical fibers. Optogenetic demonstrations in mice include place-preference and anxiety-like behavior modulation.



Similar designs but with stretchable RF energy harvesters and  $\mu$ -ILEDs in soft polymer matrices (i.e. PDMS, effective modulus of 1.7 MPa) can yield mechanics and form factors that allow the effective integration with soft biological tissues in highly mobile areas of the peripheral nervous system and the spinal cord (figure 2d).<sup>98</sup> The stretchability (strains up to 30%), the miniaturized geometry ( $\sim 16 \text{ mm}^3$ ) and the lightweight construction ( $\sim 16 \text{ mg}$ ) enable robust operation for 6 months or more after subdermal implantation, confirming reliable function under physiological strains in freely behaving animals. Optimized designs (2.34 GHz, far-field RF transmission) can reduce the antenna areas ( $3 \times 3 \text{ mm}$ ) by two orders of magnitude relative to those of conventional approaches based on battery power. The wide bandwidths (200 MHz) of such antennas further reduce the effects of slight mismatches between the central operating frequency of the antenna and the RF transmitter (figure 3a), allowing functional place aversion experiments with both the sciatic nerve and spinal cord of mice expressing Chr2.

Related embodiments support miniaturized platforms ( $0\text{-}25 \text{ mm}^3$  and  $20\text{-}50 \text{ mg}$ ) that exploit the RF resonant cavity approach described previously. The devices consist of hand wound coils,  $\mu$ -ILEDs, and circuitry for application in the premotor cortex and spinal cord (Figure 3b).<sup>122</sup> Here, the cavity (21 cm diameter, 15 cm height) generates localized electromagnetic energy (1.5 GHz) selectively coupled into the body of mice at all positions within a custom experimental cage. Functional demonstrations show increased circling locomotion and reflexive nocifensive behavior via optogenetic stimulation (blue light,  $6\text{-}40 \text{ mW/mm}^2$ ) in the right premotor cortex and spinal cord of transgenic mice expressing Thy1-ChR2-EYFP and c-Fos, respectively.

Optoelectronic devices based on near-field magnetic resonant coupling at 13.56 MHz (figure 2e) exploit flexible printed circuit board technology (copper metal traces on top and bottom of polyimide substrate) for the antenna and injectable needle, and enable wireless power transmission and positioning of the  $\mu$ -ILEDs into the deep brain. An adaptation enables optogenetic studies of the spinal cord (Figure 3c) and various parts of peripheral nervous system.<sup>100, 210</sup> As in the previous cases, miniaturized geometries ( $10 \text{ mm}^3$ ) and lightweight ( $\sim 20 \text{ mg}$ ) construction enable complete subdermal implantation without altering locomotor function or inducing anxiety-like behavior, as determined by comparisons to sham operated controls.<sup>100</sup> The designs allow for mechanical flexing with minimal changes in power transmission efficiency (change of Q factor  $< 0.12$ ) or resonance frequency ( $< 0.1 \text{ MHz}$ ) even for bending to radii of curvature of 5 mm, for reliable operation under natural deformations. Experimental demonstrations include the optical activation of TRPV1-ChR2 spinal afferents that result in a real-time place aversion in freely behaving mice.

Coordinated dissection of neuronal populations at multiple locations and selective modulation of individual subjects in social behavioral studies requires the precise control over the intensity of the stimulation and over multiple devices and multiple light emitters in a single device. These capabilities can be provided by active electronic designs with programmable simplex communication schemes enabled by binary on-off-keying protocols to send commands to the implant (Figure 3d).<sup>102</sup> The patterns of optical stimuli are achieved by a microcontroller that provides timing and illumination information for activating the  $\mu$ -ILEDs. In a specific example, the independent operation of multiple

$\mu$ -ILEDs on separate probes and four  $\mu$ -ILEDs for bilateral operation (figure 3d) allows optogenetic neuromodulation of spatially distinct sites with programmable frequencies and duty cycles. In separate embodiments, programmable and precise control over emission intensity, realized by an additional digital-to-analog (DAC) circuit that provides output frequencies as high as 1.5 kHz, can be used for in-vivo, rapid characterization of new opsins and for the interrogation of neural circuits with high temporal resolution. Active power management can be achieved with a low-dropout (LDO) linear regulator coupled with a pair of time-multiplexed antennas, to yield power harvesting performance that is invariant to position and angular orientation, as a stable DC power supply for the circuits and  $\mu$ -ILEDs. These advanced modes of operation are possible without significantly increasing the device size or weight, thereby retaining all of the attractive features associated with the form factors of the passive platforms. An additional feature of this device type is the absence of magnetic components, enabling medical imaging such as CT (computer tomography) and MRI (magnetic resonance imaging) on implanted animals. The results can provide important insights into location of the implants as well as the status of surrounding tissues in vivo.

### Photonic Therapy.

The potential for therapeutic applications of optogenetics described in previous section is of broad interest, with experimental demonstrations in animal models to restore visual function in retinitis pigmentosa,<sup>211-213</sup> to control spontaneous epileptic seizures,<sup>214, 215</sup> and to pace and resynchronization cardiac activity.<sup>216</sup> In one example, a set of wirelessly powered LEDs (far red light, 730 nm) activates photoreceptors (monophosphate synthase) that initiate insulin gene expression for the treatment of diabetes in mice (Figure 4a).<sup>217</sup> In this system, customized transmitting coils around the cage provide electromagnetic power (magnetic resonant coupling at 180 kHz) to the implant. *In vivo* experiments use wireless delivery of insulin for the rapid restoration of homeostatic blood glucose in freely moving animal subjects. A user-interface paired with a separate Bluetooth-enabled glucose monitor further enables the semi-automatic glycemia-dependent activation of a wireless power transmitter that controls the brightness of the LED and the illumination time.

Other means to exploit light-tissue interactions include photodynamic therapy (PDT), where light activates certain types of drugs or photosensitizers, to deliver pharmacological agents to highly targeted areas in a controlled fashion, ideal for long-term therapies. For example, miniaturized (15 mm<sup>3</sup>, 30 mg) optoelectronic devices wirelessly powered with RF radiation (frequencies between 1 and 1.5 GHz) activate photosensitizers (chlorin e6) through thick (> 3 cm) tissues for suppressing tumor growth in mouse cancer models (Figure 4b).<sup>218</sup> The device in this case consists of a three-turn coil for wireless power harvesting, and a rectifier to convert RF into direct current (DC) to drive two LEDs (red, 660 nm, and violet, 400 nm), encapsulated in biocompatible soft elastomer (PDMS). Although this device focuses on light actuated therapy to induce apoptosis in tumor cells, the foundational materials and engineering approaches can be adapted for other types of neural interface systems.

## Microfluidic delivery of drugs.

Devices with capabilities in pharmacological delivery provide unique opportunities for cell/tissue-specific targeting. For example optogenetic and chemogenetic systems can be combined for light dependent activation of pharmacological agent<sup>19, 221-224</sup> and deep brain stimulation for psychiatric disorders.<sup>225</sup> Conventional drug delivery systems in these models rely on metal cannulas coupled to reservoirs/micropumps via tubing, or on syringe injection, leading to disadvantages that are similar to those of tethered systems, and in most cases even more significant due to the thick, stiff tubing needed for efficient fluid delivery. Wireless powering and control strategies for compact microfluidic systems that incorporate reservoirs, valves, pumps and channels for delivery of multiple pharmacological agents to highly localized target locations (i.e., deep brain, spinal cord) are thus advantageous. The soft, microfluidic probes in these platforms adopt a multilayer architecture to support multimodal operation, with options in optical, electrical and/or chemical sensing and activation. The integrated pumps eliminate the need for external fluid handling hardware or syringe pumps.<sup>226</sup> In one example  $\mu$ -ILEDs integrate with microfluidic probes (500  $\mu\text{m}$  x 80  $\mu\text{m}$ ), compact thermally actuated pumps and associated reservoirs ( $\sim 73 \text{ mm}^3$ ), along with a dual channel RF control module ( $\sim 52 \text{ mm}^3$ , peak power transmission at 1.8 GHz and 2.9 GHz) as part of a miniaturized ( $\sim 125 \text{ mm}^3$ ), lightweight (220 mg), flexible platform (Figure 5a).<sup>227</sup> The fluid reservoir/pump exploits a thermally expandable composite material for 90% delivery efficiency in volume ( $\sim 0.46 \mu\text{L}$  from 0.5  $\mu\text{L}$  reservoir) via activation of an associated Joule heating element ( $\sim 100 \text{ }^\circ\text{C}$ ). A cyclic olefin polymer forms the structure to define the reservoirs, selected due to its low water vapor permeability ( $0.023 \text{ g mm m}^{-2} \text{ d}^{-2}$ ) for effective storage of drugs. This platform allows operation in freely behaving animals with little behavioral impact. The main disadvantages are in high power consumption of the thermal-mechanical pumping mechanism and the absence of means to refill the reservoirs for multiple cycles of use.

Recent work addresses these limitations through the use of magnetic resonant coupling for power transfer and electrochemical pumps for power efficient operation (Figure 5b).<sup>144</sup> In a version designed for interfaces to peripheral nerves, the device consists of (i) a low modulus ( $\sim 3 \text{ MPa}$ ) elastomeric cuff that surrounds a targeted nerve, (ii) four microfluidic channels (total thickness of 200  $\mu\text{m}$ , cross sectional area of  $60 \times 60 \mu\text{m}^2$ ) along the length of the probe that leads to the cuff, and (iii) an  $\mu$ -ILED integrated on the cuff for light delivery. The section of the implant responsible for wireless energy harvesting, electronic control and pumping (radius of 5 mm, thickness of  $\sim 4 \text{ mm}$ ) also stores the drugs in sealed reservoirs. Here, four electrochemical pumps ( $\sim 1.5 \mu\text{L}$ ) consume low power ( $\sim 800 \mu\text{W}$ ) in the electrolysis of water to produce pressure via the generation of oxygen and hydrogen gas, as the driving force to pump the corresponding drugs with high levels of control. The fully assembled system weighs only 0.3 g (compared to 1.8 g of the thermally actuated system with assembled battery<sup>16</sup>), resulting in minimal impact on the target subject. Experimental demonstration in freely behaving subjects with optical activation (blue, 470 nm) of excitatory neurons expressing ChR2 result in place aversion in a Y maze experiment where only one arm of the experimental enclosure involves optogenetic stimulation. Conversely, a reduction in pain threshold, specifically thermal sensitivity, can

be achieved with the delivery of bupivacaine (40 mg/ml), a local anesthetic. The soft mechanics of the cuff (PDMS) result in minimal irritation of the nerve when compared to otherwise similar structures formed with polyethylene. A relatively straightforward modification of this same platform, but with an injectable needle as support for thin and soft microfluidic channels ( $0.35 \times 0.1 \text{ mm}^2$ , modulus of 3 MPa) and  $\mu$ -ILEDs allows for use in targeted areas of the deep brain (Figure 5c).<sup>62</sup> Surgical insertion of such probe into the brain and fixation of the device (0.3 g) on top of the skull do not disrupt normal locomotion. Notably, use of such lighter and less obtrusive platforms shows substantially higher baseline locomotion compared to the battery-operated devices (1.86 g). The high degree of mechanical compliance of the probe further reduces lesioning ( $0.068 \text{ mm}^2$  compare to  $0.184 \text{ mm}^2$  via metal cannula with diameter of 0.46 mm)<sup>62</sup> and immunoreactive glial responses compared to those associated with conventional cannulas. In a demonstration experiment using this brain-interfaced optofluidic device, optical stimulation of the ventral tegmental area of wild-type mice increases locomotion behavior while concurrent wireless infusion of an N-methyl-D-aspartate (NMDA) receptor antagonist blocks this activity. The use of multiple, independently addressable reservoirs allows for multiple infusion events, for viruses or tracers that may provide additional information on neuronal circuit dynamics in combination with optogenetic stimulation.

### Bio-signal recording.

Most technologies for wireless optogenetics and pharmacology described in previous sections focus on manipulating neuronal and/or cellular activity, rather than recording or sensing. A crucial modality for the precise interpretation of behavior of the central and peripheral nervous systems and of other organs as well as for closed-loop modulation of the latter is the ability to capture physiological activities with high fidelity. Recent advances in electronics and microfabrication enable recording with on-board signal processing such as filtering, amplification, and digitization. As an example, progress in miniaturization of battery-free electronics and data communication serves as the basis for fully implantable wireless systems to measure the oxygen saturation of targeted tissue (i.e. deep brain) in freely behaving animals (Figure 6a).<sup>143</sup> Key components in this small device (lateral dimensions of  $10 \times 10 \text{ mm}^2$ , the thickness of  $\sim 0.25 \text{ mm}$ , and the weight of 0.1g) include (i) microscale optoelectronic elements ( $\mu$ -ILEDs, and a microscale inorganic photodetector ( $\mu$ -IPD)) that enable the recording of local hemoglobin dynamics, and (ii) sub-systems for continuous, wireless power delivery and data transfer. Radiometric measurements that leverage differences in absorption of hemoglobin in its oxygenated and deoxygenated state reveal oxygenation dynamics of the target tissue. The device can resolve regional tissue oxygen saturation levels in small tissue volumes defined by the illumination profiles ( $0.5$  to  $2 \text{ mm}^3$ ). The results yield insights into underlying mechanisms of regional  $\text{O}_2$ -mediated biological processes (i.e., neural activity, tissue perfusion, and wound healing),<sup>228-230</sup> with the potential to provide therapeutic guidance, real-time organ health, and closed-loop regulation of physiological processes.

Ultrasound coupled sensors attached on a peripheral nerve and a skeletal muscle can measure ENG and EMG, respectively (Figure 6b).<sup>126, 231</sup> Here, a device ( $2.4 \text{ mm}^3$ ) consists of a piezocrystal ( $\sim 0.42 \text{ mm}^3$ ), custom integrated circuit ( $0.5 \times 0.45 \text{ mm}^2$ ), and gold

recording electrodes ( $0.2 \times 0.2 \text{ mm}^2$ ), packaged within medical grade UV-curable epoxy. Data communication relies on the modulation of backscattered waves that carry analog information on the EMG and ENG signals. Initial demonstrations illustrate the recovery of ground truth action potentials with a correlation of  $\sim 90\%$ . One recent example uses related methods to enable further miniaturized neural recording implant ( $0.8 \text{ mm}^3$ ) on motor cortex of an awake behaving rat.<sup>232, 233</sup>

Combining mature silicon CMOS technologies and emerging wireless power transfer schemes provides alternative strategies for ultraminiaturized devices that can record and stimulate. An ASIC-system based on 130-nm-CMOS processes includes the recording electrodes (mixture of conductive polymer and carbon nanotube (CNT), PEDOT:PSS (poly(3,4-ethylenedioxythiophene) poly(styrenesulfonate))/CNT), a pair of composite electrodes (mixture of conductive polymer and carbon nanotube, PEDOT:PSS/CNT) integrated on the sidewalls of the CMOS die, an on-chip coil antenna for wireless power harvesting via magnetic coupling, and CMOS circuits for operation control, all integrated on a single die with a dimension of  $300 \mu\text{m} \times 300 \mu\text{m} \times 80 \mu\text{m}$  (Figure 6c). Devices of this type enable direct injection into the target areas via a syringe needle (inner diameter of  $0.4 \text{ mm}$ )<sup>146</sup> for distributed free-floating operations at multiple locations. The communication method provides sufficient bandwidth to address up to 10 different devices via a frequency division multiple access system (from 0.5 GHz to 3 GHz with 250 MHz spacing). When implanted in the sciatic nerve of a rat, the device can deliver electrical stimulation and elicit action potentials in the axons, as evidenced by the clear EMG response.

The wireless device platforms highlighted in the previous examples aim for long term bio-integration. An emerging class of technology that focuses on transient applications such as those in post-surgery monitoring require only limited operation times and benefit from device dissolution or disintegration to benign end products after a controlled period of stable operation within the body.<sup>234, 235</sup> Such types of biodegradable monitoring systems have the potential to monitor<sup>106, 236</sup> and treat<sup>237, 238</sup> a variety of conditions without the need for surgical extraction procedures. Entirely biodegradable and biocompatible electrical peripheral nerve stimulators with wirelessly operated energy harvesting systems (magnetic resonant coupling at  $\sim 5 \text{ MHz}$ ) and stimulating electrodes yield accelerated functional recovery and neuroregeneration of injured peripheral nerves in rodent models.<sup>237</sup>

### **Closed loop operation.**

Conditional (or closed-loop) operations combine sensing and actuating capabilities, with real-time signal processing and modulation for the real-time identification and control of neural disorders<sup>214</sup>, and bridging dysconnectivity in injured neural circuits.<sup>36, 239</sup> A single implantable device can be programmed to deliver stimulation when certain conditions are met (i.e. seizure onset),<sup>141, 240</sup> or multiple devices (i.e. stimulation and recording) can support a closed-loop operation through a wireless link.<sup>217, 241</sup> The discussion of conditions and basic components can be found elsewhere.<sup>242, 243</sup>

A fully implantable, wireless and battery-free optoelectronic platform with (i) a conformal optogenetic interface for stimulation of a peripheral nerve, (ii) a soft, precision biophysical

sensor for continuous measurement of organ function, and (iii) a wireless control/power module and data analytic approach for coordinated, closed-loop correction of pathological physiology in real-time (figure 7)<sup>141</sup> enables automated neuromodulation with long-term stability (> 1 month) and minimally invasive operation. For example, cell specific stimulation of sensory afferent nerves that innervate the bladder, based on continuous monitoring of bladder function with an ultra-soft, stretchable strain gauge (~80  $\mu\text{m}$  thickness) as a sensor of voiding and associated real-time data analytics to identify overactivity. Automated optogenetic neuromodulation of bladder sensory afferents with  $\mu\text{-ILEDs}$  (540nm) on a platform collocated with the strain sensor enables the regulation of bladder function in the context of acute cystitis. The closed-loop operation involves real-time, multi-step signal analysis (i.e., down-sampling, smoothing, and derivative calculation) to identify bladder voiding with > 85% and 95% accuracy for naive and cyclophosphamide inflamed bladder, respectively. Implantation in rats leads to no significant immune response or impairments in gait, movements, weight, with no adverse effects on bladder cytometric properties 7 days after implantation, compared to sham surgery animals. The data analytics and engineering approaches for this work, together with the wireless control/power module and associated interface, can be readily adapted and combined with other functional systems, such as microfluidics and photometry, to yield platforms for regulating the function of other organs.

## Conclusions

Wireless implantable medical devices can now match, and in many cases exceed, the capabilities of many types of tethered systems by integrating techniques and methods in soft materials, processing approaches, advanced wireless electronics, energy harvesting schemes and microscale interface components. Highly miniaturized platforms of this type can operate chronically in freely behaving animals across nearly any part of the anatomy, as advanced diagnostic and, therapeutic technologies for studies that require specific interfaces with various parts of the central and peripheral nervous systems. The ability to monitor and regulate physiological processes seamlessly without impact on the host animal creates important capabilities that foreshadow powerful digital health systems and engineered forms of therapies (e.g. electroceuticals or bioelectronic medicines) that can leverage complementary research efforts in material-oriented approaches (e.g. upconverting nanoparticles,<sup>1, 24, 25</sup> magnetic nanoparticles<sup>26-28</sup> and ultrasound-based contrast agents<sup>29, 30</sup>) into a multimodal system. Research and practical applications will rely on fundamental insights into neuronal characteristics where inferred models of dynamics, connectivity, and causation are accurate in untethered subjects. The technical maturity of the systems described here have evolved substantially over the last 5 years, to the point that many are now commercially available as research tools and others are in advanced stages of commercial development for use not only on animal models and cell assays, but also for human health.

Remaining challenges and associated opportunities for additional work are in chronic, in vivo operation of flexible and especially stretchable systems, where encapsulation schemes and designs at the bio-interface must be configured to reach, and preferably exceed, human lifespans. The most significant hurdles in this context are those associated with complex



systems that can provide advanced multimodal recording and stimulation capabilities, with soft mechanics. Here, improved bandwidth in wireless communication schemes, capable of relaying high-fidelity information continuously, and increased computational resources for preprocessing of information on the device will be important. Power supply will remain as a critical, related consideration, where unusual wireless power transmission infrastructures may allow for operation outside of specialized environments. Further improvements in sensing capabilities, particularly in technologies that can perform precise biochemical analyses, will add to an increasing volume of data, with strong potential value when coupled to emerging techniques in machine learning and artificial intelligence.

## Acknowledgements

L.C. and P.G. acknowledge the support of the Improving Health TRIF Project. P.G. acknowledges the support of NIG-NINDS R01NS112535 and start-up funds from the Department of Biomedical Engineering at the University of Arizona. S.M.W. acknowledges the support of the MSIT (Ministry of Science and ICT), Korea, under the ICT Creative Consilience program (IITP-2020-0-01821), supervised by the IITP (Institute for Information & communications Technology Planning & Evaluation). S.M.W. acknowledges support by a National Research Foundation of Korea (NRF) grant funded by the Korea government (MSIP; Ministry of Science, ICT & Future Planning; grant no. 2020R1G1A1101267). S.M.W. acknowledges the support by Nano Material Technology Development Program (2020M3H4A1A03084600) through the National Research Foundation of Korea (NRF) funded by the Ministry of Science and ICT of Korea.

## Reference

- Rivnay J, LWang H, Fenno L, Delsseroth K & Mallaras GG Next-generation probes, particles, and proteins for neural interfacing. *Sci. Adv* 3, e1601649 (2017). [PubMed: 28630894]
- Hong G & Lieber CM Novel electrode technologies for neural recordings. *Nat. Rev. Neurosci* 20, 330–345 (2019). [PubMed: 30833706]
- Jeong JW et al. Soft materials in neuroengineering for hard problems in neuroscience. *Neuron* 86, 175–186 (2015). [PubMed: 25856493]
- Tybrandt K et al. High-density stretchable electrode grids for chronic neural recording. *Adv. Mater* 30, e1706520 (2018). [PubMed: 29488263]
- Won SM et al. Recent advances in materials, devices, and systems for neural interfaces. *Adv. Mater* 30, e1800534 (2018). [PubMed: 29855089]
- Azevedo CA & Mammis A Neuromodulation therapies for alcohol addiction: a literature review. *Neuromodulation* 21, 144–148 (2018). [PubMed: 28055126]
- Bouthour W et al. Biomarkers for closed-loop deep brain stimulation in Parkinson disease and beyond. *Nat. Rev. Neurol* 15, 343–352 (2019). [PubMed: 30936569]
- Fang JY & Tolleson C The role of deep brain stimulation in Parkinson's disease: an overview and update on new developments. *Neuropsychiatr. Dis. Treat* 13, 723–732 (2017). [PubMed: 28331322]
- Kuo CH, White-Dzuro GA & Ko AL Approaches to closed-loop deep brain stimulation for movement disorders. *Neurosurg. Focus* 45, E2 (2018).
- Wellman SM et al. A materials roadmap to functional neural interface design. *Adv. Funct. Mater* 28, 1701269 (2018). [PubMed: 29805350]
- Robinson JT, Jorgolli M & Park H Nanowire electrodes for high-density stimulation and measurement of neural circuits. *Front Neural Circuits* 7, 38 (2013). [PubMed: 23486552]
- Fan B & Li W Miniaturized optogenetic neural implants: a review. *Lab Chip* 15, 3838–3855 (2015). [PubMed: 26308721]
- Fu R et al. Implantable and biodegradable poly(l-lactic acid) fibers for optical neural interfaces. *Adv. Opt. Mater* 6 (2018).
- Gutruf P & Rogers JA Implantable, wireless device platforms for neuroscience research. *Curr. Opin. Neurobiol* 50, 42–49 (2018). [PubMed: 29289027]

15. Park S, Loke G, Fink Y & Anikeeva P Flexible fiber-based optoelectronics for neural interfaces. *Chem. Soc. Rev* 48, 1826–1852 (2019). [PubMed: 30815657]
16. Jeong JW et al. Wireless optofluidic systems for programmable in vivo pharmacology and optogenetics. *Cell* 162, 662–674 (2015). [PubMed: 26189679]
17. Pons-Faudoa FP, Ballerini A, Sakamoto J & Grattoni A Advanced implantable drug delivery technologies: transforming the clinical landscape of therapeutics for chronic diseases. *Biomed. Microdevices* 21, 47 (2019). [PubMed: 31104136]
18. Sanjay ST et al. Recent advances of controlled drug delivery using microfluidic platforms. *Adv. Drug Deliv. Rev* 128, 3–28 (2018). [PubMed: 28919029]
19. Sim JY, Haney MP, Park SI, McCall JG & Jeong JW Microfluidic neural probes: in vivo tools for advancing neuroscience. *Lab Chip* 17, 1406–1435 (2017). [PubMed: 28349140]
20. Liu Y et al. Soft and elastic hydrogel-based microelectronics for localized low-voltage neuromodulation. *Nat. Biomed. Eng* 3, 58–68 (2019). [PubMed: 30932073]
21. Zhang Y et al. Climbing-inspired twining electrodes using shape memory for peripheral nerve stimulation and recording. *Sci. Adv* 5, eaaw1066 (2019). [PubMed: 31086809]
22. Opie NL et al. Focal stimulation of the sheep motor cortex with a chronically implanted minimally invasive electrode array mounted on an endovascular stent. *Nat. Biomed. Eng* 2, 907–914 (2018). [PubMed: 31015727]
23. Yan Z et al. Three-dimensional mesostructures as high-temperature growth templates, electronic cellular scaffolds, and self-propelled microrobots. *Proc. Natl. Acad. Sci. USA* 114, E9455–E9464 (2017). [PubMed: 29078394]
24. All AH et al. Expanding the toolbox of upconversion nanoparticles for in vivo optogenetics and neuromodulation. *Adv. Mater* 31, e1803474 (2019). [PubMed: 31432555]
25. Chen S et al. Near-infrared deep brain stimulation via upconversion nanoparticle-mediated optogenetics. *Science* 359, 679–684 (2018). [PubMed: 29439241]
26. Christiansen MG, Senko AW & Anikeeva P Magnetic strategies for nervous system control. *Annu. Rev. Neurosci* 42, 271–293 (2019). [PubMed: 30939100]
27. Roet M et al. Progress in neuromodulation of the brain: a role for magnetic nanoparticles? *Prog. Neurobiol* 177, 1–14 (2019). [PubMed: 30878723]
28. Chen R, Romero G, Christiansen MG, Mohr A & Anikeeva P Wireless magnetothermal deep brain stimulation. *Science* 347, 1477–1480 (2015). [PubMed: 25765068]
29. Chu PC et al. Neuromodulation accompanying focused ultrasound-induced blood-brain barrier opening. *Sci. Rep* 5, 15477 (2015). [PubMed: 26490653]
30. Blackmore J, Shrivastava S, Sallet J, Butler CR & Cleveland RO Ultrasound neuromodulation: a review of results, mechanisms and safety. *Ultrasound Med. Biol* 45, 1509–1536 (2019). [PubMed: 31109842]
31. Farra R et al. First-in-human testing of a wirelessly controlled drug delivery microchip. *Sci. Transl. Med* 4, 122ra121 (2012).
32. Abraham WT et al. Wireless pulmonary artery haemodynamic monitoring in chronic heart failure: a randomised controlled trial. *Lancet*. 377, 658–666 (2011). [PubMed: 21315441]
33. Stingl K et al. Artificial vision with wirelessly powered subretinal electronic implant alpha-IMS. *Proc. Biol. Sci* 280, 20130077 (2013). [PubMed: 23427175]
34. Borton DA, Yin M, Aceros J & Nurmikko A An implantable wireless neural interface for recording cortical circuit dynamics in moving primates. *J. Neural Eng* 10, 026010 (2013). [PubMed: 23428937]
35. Finkelstein A et al. Three-dimensional head-direction coding in the bat brain. *Nature* 517, 159–164 (2015). [PubMed: 25470055]
36. Liu X, Lu Y, Iseri E, Shi Y & Kuzum D A compact closed-loop optogenetics system based on artifact-free transparent graphene electrodes. *Front. Neurosci* 12, 132 (2018). [PubMed: 29559885]
37. Martinez D et al. Adaptive quantization of local field potentials for wireless implants in freely moving animals: an open-source neural recording device. *J. Neural Eng* 15, 025001 (2018). [PubMed: 29219118]

38. Matsushita K et al. A fully implantable wireless ECoG 128-channel recording device for human brain-machine interfaces: W-HERBS. *Front Neurosci.* 12, 511 (2018). [PubMed: 30131666]
39. Wentz CT et al. A wirelessly powered and controlled device for optical neural control of freely-behaving animals. *J. Neural Eng* 8, 046021 (2011). [PubMed: 21701058]
40. Agrawal DR et al. Conformal phased surfaces for wireless powering of bioelectronic microdevices. *Nat. Biomed. Eng* 1, 0043 (2017). [PubMed: 29226018]
41. Ferguson JE & Redish AD Wireless communication with implanted medical devices using the conductive properties of the body. *Expert Rev. Med. Devices* 8, 427–433 (2011). [PubMed: 21728728]
42. Ledet EH, Liddle B, Kradinova K & Harper S Smart implants in orthopedic surgery, improving patient outcomes: a review. *Innov. Entrep. Health* 5, 41–51 (2018). [PubMed: 30246037]
43. Tokuda T et al. 1 mm<sup>3</sup>-sized optical neural stimulator based on CMOS integrated photovoltaic power receiver. *AIP Advances* 8, 045018 (2018).
44. Yang W, Khan W, Wu J & Li W Single-channel opto-neurostimulators: a review. *J. Micromech. Microeng* 29, 043001 (2019).
45. Boyden ES, Zhang F, Bamberg E, Nagel G & Deisseroth K Millisecond-timescale, genetically targeted optical control of neural activity. *Nat. Neurosci* 8, 1263–1268 (2005). [PubMed: 16116447]
46. Deisseroth K Optogenetics. *Nat. Methods* 8, 26–29 (2011). [PubMed: 21191368]
47. Pisanello F et al. Dynamic illumination of spatially restricted or large brain volumes via a single tapered optical fiber. *Nat. Neurosci* 20, 1180–1188 (2017). [PubMed: 28628101]
48. Canales A et al. Multifunctional fibers for simultaneous optical, electrical and chemical interrogation of neural circuits in vivo. *Nat. Biotechnol* 33, 277–284 (2015). [PubMed: 25599177]
49. Gunaydin LA et al. Natural neural projection dynamics underlying social behavior. *Cell* 157, 1535–1551 (2014). [PubMed: 24949967]
50. Kim CK et al. Simultaneous fast measurement of circuit dynamics at multiple sites across the mammalian brain. *Nat. Methods* 13, 325–328 (2016). [PubMed: 26878381]
51. Piatkevich KD et al. A robotic multidimensional directed evolution approach applied to fluorescent voltage reporters. *Nat. Chem. Biol* 14, 352–360 (2018). [PubMed: 29483642]
52. Pisano F et al. Depth-resolved fiber photometry with a single tapered optical fiber implant. *Nature Methods* 16, 1185–1192 (2019). [PubMed: 31591577]
53. Wu F et al. Monolithically integrated  $\mu$ LEDs on Silicon neural probes for high-resolution optogenetic studies in behaving animals. *Neuron* 88, 1136–1148 (2015). [PubMed: 26627311]
54. Ghosh KK et al. Miniaturized integration of a fluorescence microscope. *Nat. Methods* 8, 871–878 (2011). [PubMed: 21909102]
55. Resendez SL et al. Visualization of cortical, subcortical and deep brain neural circuit dynamics during naturalistic mammalian behavior with head-mounted microscopes and chronically implanted lenses. *Nat. Protoc* 11, 566–597 (2016). [PubMed: 26914316]
56. Mineev IR et al. Electronic dura mater for long-term multimodal neural interfaces. *Science* 347, 159–163 (2015). [PubMed: 25574019]
57. Gilletti A & Muthuswamy J Brain micromotion around implants in the rodent somatosensory cortex. *J. Neural Eng* 3, 189–195 (2006). [PubMed: 16921202]
58. Sridharan A, Rajan SD & Muthuswamy J Long-term changes in the material properties of brain tissue at the implant-tissue interface. *J. Neural Eng* 10, 066001 (2013). [PubMed: 24099854]
59. Fan D et al. A Wireless Multi-Channel Recording System for Freely Behaving Mice and Rats. *Plos One* 6, e22033 (2011). [PubMed: 21765934]
60. Lu L et al. Wireless optoelectronic photometers for monitoring neuronal dynamics in the deep brain. *Proc. Natl. Acad. Sci. USA* 115, E1374–E1383 (2018). [PubMed: 29378934]
61. Zhou A et al. A wireless and artefact-free 128-channel neuromodulation device for closed-loop stimulation and recording in non-human primates. 3, 15 (2019).
62. Zhang Y et al. Battery-free, lightweight, injectable microsystem for in vivo wireless pharmacology and optogenetics. *Proc. Natl. Acad. Sci. USA* 116, 21427–21437 (2019). [PubMed: 31601737]

63. Zhang W & Yartsev MM Correlated Neural Activity across the Brains of Socially Interacting Bats. *Cell* 178, 413–428 e422 (2019). [PubMed: 31230710]
64. Jurgens U & Hage SR Telemetric recording of neuronal activity. *Methods* 38, 195–201 (2006). [PubMed: 16497514]
65. Stoodley CJ et al. Altered cerebellar connectivity in autism and cerebellar-mediated rescue of autism-related behaviors in mice. *Nat Neurosci* 20, 1744–1751 (2017). [PubMed: 29184200]
66. Wyart C et al. Optogenetic dissection of a behavioural module in the vertebrate spinal cord. *Nature* 461, 407–410 (2009). [PubMed: 19759620]
67. Endo H et al. Wireless enzyme sensor system for real-time monitoring of blood glucose levels in fish. *Biosensors and Bioelectronics* 24, 1417–1423 (2009). [PubMed: 18929477]
68. M. YM & Ulanovsky N Representation of three-dimensional space in the hippocampus of flying bats. *Science* 340, 367–372 (2013). [PubMed: 23599496]
69. Roberts TF, Gobes SM, Murugan M, Olveczky BP & Mooney R Motor circuits are required to encode a sensory model for imitative learning. *Nat. Neurosci* 15, 1454–1459 (2012). [PubMed: 22983208]
70. Kouhani MHM, Luo R, Madi F, Weber AJ & Li W in 2018 40th Annual International Conference of the IEEE Engineering in Medicine and Biology Society (EMBC) 3366–3369 (2018).
71. Gagnon-Turcotte G et al. A wireless headstage for combined optogenetics and multichannel electrophysiological recording. *IEEE Trans. Biomed. Circuits Syst* 11, 1–14 (2017). [PubMed: 27337721]
72. Gutruf P, Good CH & Rogers JA Perspective: Implantable optical systems for neuroscience research in behaving animal models—Current approaches and future directions. *J. APL Photonics* 3, 120901 (2018).
73. Lacour SP, Courtine G & Guck J Materials and technologies for soft implantable neuroprostheses. *Nat Rev Mater* 1 (2016).
74. Chen R, Canales A & Anikeeva P Neural recording and modulation technologies. *Nat Rev Mater* 2 (2017).
75. Kozai TDY, Jaquins-Gerstl AS, Vazquez AL, Michael AC & Cui XT Brain Tissue Responses to Neural Implants Impact Signal Sensitivity and Intervention Strategies. *Acs Chem Neurosci* 6, 48–67 (2015). [PubMed: 25546652]
76. Salatino JW, Ludwig KA, Kozai TDY & Purcell EK Glial responses to implanted electrodes in the brain. *Nat Biomed Eng* 1, 862–877 (2017). [PubMed: 30505625]
77. Rogers JA, Someya T & Huang YG Materials and Mechanics for Stretchable Electronics. *Science* 327, 1603–1607 (2010). [PubMed: 20339064]
78. Veisheh O et al. Size- and shape-dependent foreign body immune response to materials implanted in rodents and non-human primates. *Nat Mater* 14, 643–U125 (2015). [PubMed: 25985456]
79. Schiavone G & Lacour SP Conformable bioelectronic interfaces: Mapping the road ahead. *Science Translational Medicine* 11 (2019).
80. Vitale F et al. Fluidic Microactuation of Flexible Electrodes for Neural Recording. *Nano Lett* 18, 326–335 (2018). [PubMed: 29220192]
81. Du ZJ et al. Ultrasoft microwire neural electrodes improve chronic tissue integration. *Acta Biomater* 53, 46–58 (2017). [PubMed: 28185910]
82. Luan L et al. Ultraflexible nanoelectronic probes form reliable, glial scar-free neural integration. *Sci Adv* 3 (2017).
83. Sekitani T & Someya T Stretchable, large-area organic electronics. *Advanced Materials* 22, 2228–2246 (2010). [PubMed: 20229571]
84. Kim DH, Xiao JL, Song JZ, Huang YG & Rogers JA Stretchable, Curvilinear Electronics Based on Inorganic Materials. *Advanced Materials* 22, 2108–2124 (2010). [PubMed: 20564250]
85. Oh JY et al. Intrinsically stretchable and healable semiconducting polymer for organic transistors. *Nature* 539, 411 (2016). [PubMed: 27853213]
86. Kaltenbrunner M et al. An ultra-lightweight design for imperceptible plastic electronics. *Nature* 499, 458–463 (2013). [PubMed: 23887430]

87. Jang H et al. Graphene-Based Flexible and Stretchable Electronics. *Advanced Materials* 28, 4184–4202 (2016). [PubMed: 26728114]
88. Wang SH et al. Skin electronics from scalable fabrication of an intrinsically stretchable transistor array. *Nature* 555, 83–+ (2018). [PubMed: 29466334]
89. Sun YG, Choi WM, Jiang HQ, Huang YGY & Rogers JA Controlled buckling of semiconductor nanoribbons for stretchable electronics. *Nat Nanotechnol* 1, 201–207 (2006). [PubMed: 18654187]
90. Zhang YH et al. Mechanics of ultra-stretchable self-similar serpentine interconnects. *Acta Mater* 61, 7816–7827 (2013).
91. Qiang Y et al. Transparent arrays of bilayer-nanomesh microelectrodes for simultaneous electrophysiology and two-photon imaging in the brain. *Sci Adv* 4 (2018).
92. de la Oliva N, Mueller M, Stieglitz T, Navarro X & del Valle J On the use of Parylene C polymer as substrate for peripheral nerve electrodes. *Sci Rep-Uk* 8 (2018).
93. Viventi J et al. A Conformal, Bio-Interfaced Class of Silicon Electronics for Mapping Cardiac Electrophysiology. *Science Translational Medicine* 2 (2010).
94. Viventi J et al. Flexible, foldable, actively multiplexed, high-density electrode array for mapping brain activity in vivo. *Nat Neurosci* 14, 1599–U1138 (2011). [PubMed: 22081157]
95. Xu S et al. Soft Microfluidic Assemblies of Sensors, Circuits, and Radios for the Skin. *Science* 344, 70–74 (2014). [PubMed: 24700852]
96. Kim D-H et al. Epidermal electronics. *Sciences* 333, 838–843 (2011).
97. Lee S et al. Ultrasoft electronics to monitor dynamically pulsing cardiomyocytes. *Nat. Nanotechnol* 14, 156–160 (2019). [PubMed: 30598525]
98. Park SI et al. Soft, stretchable, fully implantable miniaturized optoelectronic systems for wireless optogenetics. *Nat. Biotechnol* 33, 1280–1286 (2015). [PubMed: 26551059]
99. Kim TI et al. Injectable, cellular-scale optoelectronics with applications for wireless optogenetics. *Science* 340, 211–216 (2013). [PubMed: 23580530]
100. Shin G et al. Flexible near-field wireless optoelectronics as subdermal implants for broad applications in optogenetics. *Neuron* 93, 509–521 (2017). [PubMed: 28132830]
101. Park SI et al. Stretchable multichannel antennas in soft wireless optoelectronic implants for optogenetics. *Proc. Natl. Acad. Sci. USA* 113, E8169–E8177 (2016). [PubMed: 27911798]
102. Gutruf P et al. Fully implantable optoelectronic systems for battery-free, multimodal operation in neuroscience research. *Nat. Electronics* 1, 652–660 (2018).
103. Xu S et al. Stretchable batteries with self-similar serpentine interconnects and integrated wireless recharging systems. *Nat Commun* 4 (2013).
104. Kim J et al. Epidermal Electronics with Advanced Capabilities in Near-Field Communication. *Small* 11, 906–912 (2015). [PubMed: 25367846]
105. Kim DH, Ghaffari R, Lu NS & Rogers JA Flexible and Stretchable Electronics for Biointegrated Devices. *Annu Rev Biomed Eng* 14, 113–128 (2012). [PubMed: 22524391]
106. Kang SK et al. Bioresorbable silicon electronic sensors for the brain. *Nature* 530, 71–76 (2016). [PubMed: 26779949]
107. Scholten K & Meng E A review of implantable biosensors for closed-loop glucose control and other drug delivery applications. *Int J Pharmaceut* 544, 319–334 (2018).
108. Scholten K & Meng E Materials for microfabricated implantable devices: a review. *Lab on a Chip* 15, 4256–4272 (2015). [PubMed: 26400550]
109. Hassler C, Boretius T & Stieglitz T Polymers for Neural Implants. *J Polym Sci Pol Phys* 49, 18–33 (2011).
110. Joung YH Development of implantable medical devices: from an engineering perspective. *Int. Neurorol. J* 17, 98–106 (2013). [PubMed: 24143287]
111. Fang H et al. Ultrathin, transferred layers of thermally grown silicon dioxide as biofluid barriers for biointegrated flexible electronic systems. *Proc. Natl. Acad. Sci. USA* 113, 11682–11687 (2016). [PubMed: 27791052]
112. Song E, Li J & Rogers JA Barrier materials for flexible bioelectronic implants with chronic stability—Current approaches and future directions. *APL Materials* 7 (2019).

113. Hashimoto M, Hata A, Miyata T & Hirase H Programmable wireless light-emitting diode stimulator for chronic stimulation of optogenetic molecules in freely moving mice. *Neurophotonics* 1, 011002 (2014). [PubMed: 26157963]
114. Gagnon-Turcotte G et al. A Wireless optogenetic headstage with multichannel electrophysiological recording capability. *Sensors* 15, 22776–22797 (2015). [PubMed: 26371006]
115. Mei H & Irazoqui PP Miniaturizing wireless implants. *Nat Biotechnol* 32, 1008–1010 (2014). [PubMed: 25299922]
116. Ben Amar A, Kouki AB & Cao H Power approaches for implantable medical devices. *Sensors* 15, 28889–28914 (2015). [PubMed: 26580626]
117. Wang J, He T & Lee C Development of neural interfaces and energy harvesters towards self-powered implantable systems for healthcare monitoring and rehabilitation purposes. *Nano Energy* 65 (2019).
118. Hwang G-T et al. Self-powered deep brain stimulation via a flexible PIMNT energy harvester. *Energy Environ. Sci* 8, 2677–2684 (2015).
119. Yao G et al. Effective weight control via an implanted self-powered vagus nerve stimulation device. *Nat. Commun* 9, 5349 (2018). [PubMed: 30559435]
120. Bullen RA, Arnot TC, Lakeman JB & Walsh FC Biofuel cells and their development. *Biosens. Bioelectron* 21, 2015–2045 (2006). [PubMed: 16569499]
121. Settaluri KT, Lo H & Ram RJ Thin thermoelectric generator system for body energy harvesting. *J. Electron. Mater* 41, 984–988 (2012).
122. Montgomery KL et al. Wirelessly powered, fully internal optogenetics for brain, spinal and peripheral circuits in mice. *Nature Methods* 12, 969–974 (2015). [PubMed: 26280330]
123. Lee S et al. A 250  $\mu\text{m}$  x 57  $\mu\text{m}$  microscale opto-electronically transduced electrodes (MOTEs) for neural recording. *IEEE Trans. Biomed. Circuits Syst* 12, 1256–1266 (2018). [PubMed: 30334768]
124. Ding H et al. Microscale optoelectronic infrared-to-visible upconversion devices and their use as injectable light sources. *Proc. Natl. Acad. Sci. USA* 115, 6632–6637 (2018). [PubMed: 29891705]
125. Charthad J, Weber MJ, Chang TC & Arbabian A A mm-sized implantable medical device (IMD) with ultrasonic power transfer and a hybrid bi-directional data link. *IEEE J. of Solid-State Circuits* 50, 1741–1753 (2015).
126. Seo D et al. Wireless recording in the peripheral nervous system with ultrasonic neural dust. *Neuron* 91, 529–539 (2016). [PubMed: 27497221]
127. Rezaei M, Maghsoudloo E, Bories C, De Koninck Y & Gosselin B A Low-Power Current-Reuse Analog Front-End for High-Density Neural Recording Implants. *Ieee T Biomed Circ S* 12, 271–280 (2018).
128. Park SY, Cho J, Lee K & Yoon E Dynamic Power Reduction in Scalable Neural Recording Interface Using Spatiotemporal Correlation and Temporal Sparsity of Neural Signals. *Ieee J Solid-St Circ* 53, 1102–1114 (2018).
129. Wu X et al. in 2018 IEEE Symposium on VLSI Circuits 191–192 (IEEE, 2018).
130. Schwarz DA et al. Chronic, wireless recordings of large-scale brain activity in freely moving rhesus monkeys. *Nature Methods* 11, 670 (2014). [PubMed: 24776634]
131. Burton A et al. Wireless, battery-free subdermally implantable photometry systems for chronic recording of neural dynamics. (2020).
132. Sivaji V et al. ReStore: A wireless peripheral nerve stimulation system. *J Neurosci Meth* 320, 26–36 (2019).
133. Dagdeviren C et al. Conformal piezoelectric energy harvesting and storage from motions of the heart, lung, and diaphragm. *Proc. Natl. Acad. Sci. USA* 111, 1927–1932 (2014). [PubMed: 24449853]
134. Ouyang H et al. Symbiotic cardiac pacemaker. *Nat. Commun* 10, 1821 (2019). [PubMed: 31015519]



135. Falk M, Villarrubia CWN, Babanova S, Atanassov P & Shleev S Biofuel Cells for Biomedical Applications: Colonizing the Animal Kingdom. *Chemphyschem* 14, 2045–2058 (2013). [PubMed: 23460490]
136. Rapoport BI, Kedzierski JT & Sarpeshkar R A glucose fuel cell for implantable brain-machine interfaces. *PLoS One* 7, e38436 (2012). [PubMed: 22719888]
137. Mercier PP, Lysaght AC, Bandyopadhyay S, Chandrakasan AP & Stankovic KM Energy extraction from the biologic battery in the inner ear. *Nat Biotechnol* 30, 1240 (2012). [PubMed: 23138225]
138. Schroeder TBH et al. An electric-eel-inspired soft power source from stacked hydrogels. *Nature* 552, 214+ (2017). [PubMed: 29239354]
139. Nan KW et al. Compliant and stretchable thermoelectric coils for energy harvesting in miniature flexible devices. *Sci Adv* 4 (2018).
140. Kim A, Ochoa M, Rahimi R & Ziaie B New and Emerging Energy Sources for Implantable Wireless Microdevices. *Ieee Access* 3, 89–98 (2015).
141. Mickle AD et al. A wireless closed-loop system for optogenetic peripheral neuromodulation. *Nature* 565, 361–365 (2019). [PubMed: 30602791]
142. Obaid S & Lu LY Highly Efficient Microscale Gallium Arsenide Solar Cell Arrays as optogenetic Power Options. *Ieee Photonics J* 11 (2019).
143. Zhang H et al. Wireless, battery-free optoelectronic systems as subdermal implants for local tissue oximetry. *Sci. Adv* 5, eaaw0873 (2019). [PubMed: 30873435]
144. Zhang Y et al. Battery-free, fully implantable optofluidic cuff system for wireless optogenetic and pharmacological neuromodulation of peripheral nerves. *Sci. Adv* 5, eaaw5296 (2019). [PubMed: 31281895]
145. Jia YY, Wang ZY, Mirbozorgi SA & Ghovanloo M A Closed-Loop Wireless Homecage for Optogenetic Stimulation Experiments. *Biomed Circ Syst C*, 426–429 (2015).
146. Khalifa A et al. The Microbead: A 0.009 mm<sup>3</sup> implantable wireless neural stimulator. *IEEE Trans. Biomed. Circuits Syst* (2019).
147. Dagdeviren C et al. Flexible piezoelectric devices for gastrointestinal motility sensing. *Nat. Biomed. Eng* 1, 807–817 (2017). [PubMed: 31015594]
148. Dagdeviren C et al. Recent progress in flexible and stretchable piezoelectric devices for mechanical energy harvesting, sensing and actuation. *Extreme Mech. Lett* 9, 269–281 (2016).
149. El Ichi-Ribault S et al. Remote wireless control of an enzymatic biofuel cell implanted in a rabbit for 2 months. *Electrochimica Acta* 269, 360–366 (2018).
150. Dong K et al. Microbial fuel cell as power supply for implantable medical devices: a novel configuration design for simulating colonic environment. *Biosens. Bioelectron* 41, 916–919 (2013). [PubMed: 23122754]
151. Gonzalez-Solino C & Lorenzo MD Enzymatic Fuel Cells: Towards Self-Powered Implantable and Wearable Diagnostics. *Biosensors (Basel)* 8, 11 (2018). [PubMed: 29382147]
152. Rasmussen M, Ritzmann RE, Lee I, Pollack AJ & Scherson D An Implantable Biofuel Cell for a Live Insect. *J Am Chem Soc* 134, 1458–1460 (2012). [PubMed: 22239249]
153. Halamkova L et al. Implanted Biofuel Cell Operating in a Living Snail. *J Am Chem Soc* 134, 5040–5043 (2012). [PubMed: 22401501]
154. Castorena-Gonzalez JA et al. Biofuel Cell Operating in Vivo in Rat. *Electroanal* 25, 1579–1584 (2013).
155. Zebda A et al. Challenges for successful implantation of biofuel cells. *Bioelectrochemistry* 124, 57–72 (2018). [PubMed: 30007207]
156. Yu X et al. Skin-integrated wireless haptic interfaces for virtual and augmented reality. *Nature* (2019).
157. Merli F et al. Design, realization and measurements of a miniature antenna for implantable wireless communication systems. *IEEE Trans. Antennas Propag* 59, 3544–3555 (2011).
158. Park SI et al. Ultraminiaturized photovoltaic and radio frequency powered optoelectronic systems for wireless optogenetics. *J. Neural Eng* 12, 056002 (2015). [PubMed: 26193450]

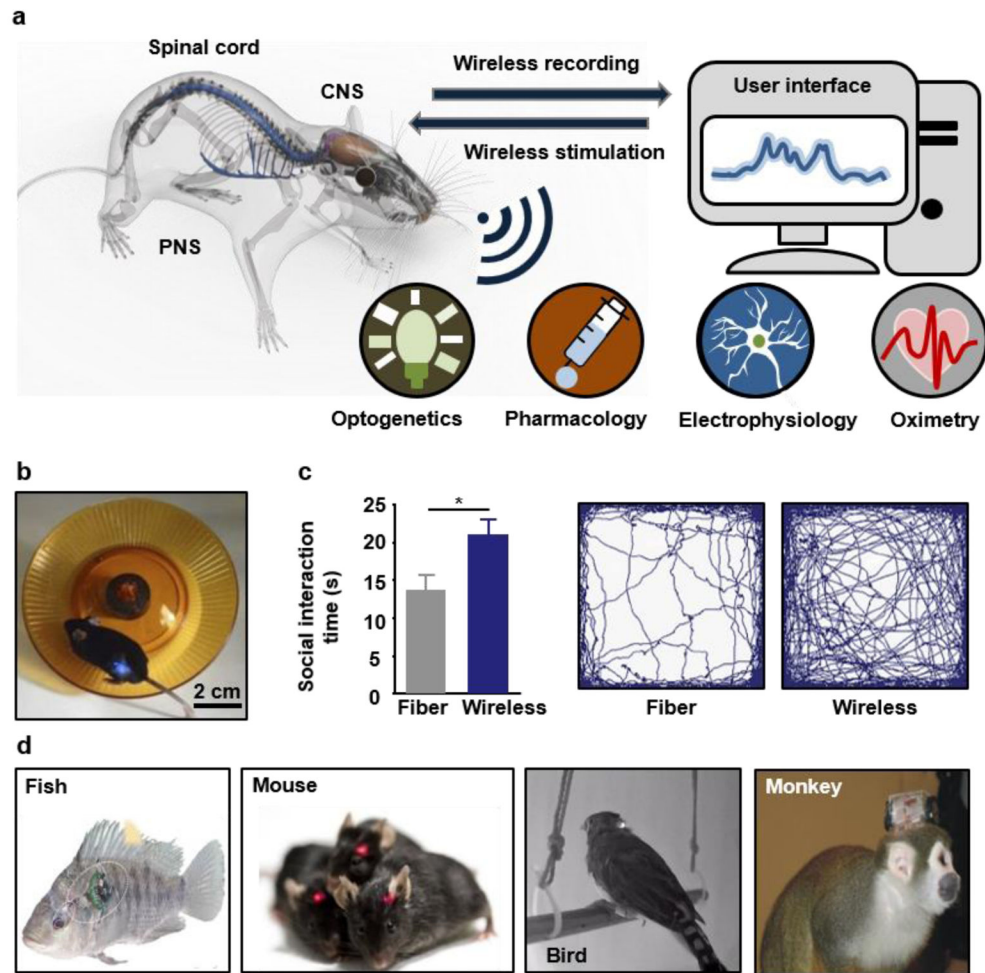
159. Xie Z, Avila R, Huang Y & Rogers JA Flexible and stretchable antennas for biointegrated electronics. *Adv. Mater*, e1902767 (2019). [PubMed: 31490582]
160. Dobkin DM *The RF in RFID: UHF RFID in practice*. (Newnes, 2012).
161. Ho JS et al. Self-tracking energy transfer for neural stimulation in untethered mice. *Physical Review Applied* 4, 024001 (2015).
162. Elder JA & Cahill DF *Biological effects of radiofrequency radiation*. Research Triangle Park, NC: U.S. Environmental Protection Agency. (1984).
163. Marincic AS Tesla, Nikola and the Wireless Transmission of Energy. *Ieee T Power Ap Syst* 101, 4064–4068 (1982).
164. Tesla N Apparatus for transmitting electrical energy. U.S. Patent 1,119,732; 1914
165. Das Barman S, Reza AW, Kumar N, Karim ME & Munir A Wireless powering by magnetic resonant coupling: Recent trends in wireless power transfer system and its applications. *Renew Sust Energ Rev* 51, 1525–1552 (2015).
166. Sallan J, Villa JL, Llombart A & Sanz JF Optimal Design of ICPT Systems Applied to Electric Vehicle Battery Charge. *Ieee T Ind Electron* 56, 2140–2149 (2009).
167. Kalwar KA, Aamir M & Mekhilef S Inductively coupled power transfer (ICPT) for electric vehicle charging - A review. *Renew Sust Energ Rev* 47, 462–475 (2015).
168. Fareq M, Fitra M, Irwanto M, Hasan S & Arinal M in *Journal of Physics: Conference Series*, Vol. 495 012019 (IOP Publishing, 2014).
169. Kurs A et al. Wireless power transfer via strongly coupled magnetic resonances. *Science* 317, 83–86 (2007). [PubMed: 17556549]
170. Ho SL, Wang JH, Fu WN & Sun MG A Comparative Study Between Novel Witricity and Traditional Inductive Magnetic Coupling in Wireless Charging. *Ieee T Magn* 47, 1522–1525 (2011).
171. Low ZN, Chinga RA, Tseng R & Lin JS Design and Test of a High-Power High-Efficiency Loosely Coupled Planar Wireless Power Transfer System. *Ieee T Ind Electron* 56, 1801–1812 (2009).
172. Zhang YM, Zhao ZM & Chen KN Frequency Decrease Analysis of Resonant Wireless Power Transfer. *Ieee T Power Electr* 29, 1058–1063 (2014).
173. Yoon IJ & Ling H Investigation of Near-Field Wireless Power Transfer in the Presence of Lossy Dielectric Materials (vol 61, pg 482, 2013). *Ieee T Antenn Propag* 61, 1016–1016 (2013).
174. Poon ASY, O'Driscoll S & Meng TH Optimal Frequency for Wireless Power Transmission Into Dispersive Tissue. *Ieee T Antenn Propag* 58, 1739–1750 (2010).
175. Cecil S et al. in *2010 Second International Workshop on Near Field Communication* 65–70 (IEEE, 2010).
176. Chung HU et al. Binodal, wireless epidermal electronic systems with in-sensor analytics for neonatal intensive care. *Science* 363, eaau0780 (2019). [PubMed: 30819934]
177. Kim J et al. Miniaturized Flexible Electronic Systems with Wireless Power and Near-Field Communication Capabilities. *Advanced Functional Materials* 25, 4761–4767 (2015).
178. Lazaro A, Villarino R & Girbau D A Survey of NFC Sensors Based on Energy Harvesting for IoT Applications. *Sensors* 18 (2018).
179. Ray TR et al. Bio-Integrated Wearable Systems: A Comprehensive Review. *Chem Rev* 119, 5461–5533 (2019). [PubMed: 30689360]
180. Hui SYR, Zhong W & Lee CK A critical review of recent progress in mid-range wireless power transfer. *IEEE Trans. Power Electron.* 29, 4500–4511 (2014).
181. Denisov A & Yeatman E in *2010 International Conference on Body Sensor Networks* 84–89 (2010).
182. Podgorski K & Ranganathan G.J.J.o.n. Brain heating induced by near-infrared lasers during multiphoton microscopy. *116*, 1012–1023 (2016).
183. Mialhe P, Mouhamed S & Haydar AJRe. The solar cell output power dependence on the angle of incident radiation. *1*, 519–521 (1991).
184. Johnson BC et al. StimDust: a 6.5 mm<sup>3</sup>, wireless ultrasonic peripheral nerve stimulator with 82% peak chip efficiency. in *2018 IEEE Custom Integrated Circuits Conference (CICC)*, 1–4 (2018).

185. Piech DK, Johnson BC, Shen K, Ghanbari MM, Li KY, Neely RM, Kay JE, Carmena JM, Maharbiz MM and Muller R A wireless millimetre-scale implantable neural stimulator with ultrasonically powered bidirectional communication. *Nature Biomedical Engineering*, 4, 207–222, 2020.
186. Basaeri H, Christensen DB, Roundy SJS & Structures A review of acoustic power transfer for bio-medical implants. 25, 123001 (2016).
187. Seo D et al. Ultrasonic beamforming system for interrogating multiple implantable sensors. *Proc. IEEE Eng. Med. Biol. Soc*, 2673–2676 (2015).
188. Administration, F.D. Guidance for industry and FDA staff information for manufacturers seeking marketing clearance of diagnostic ultrasound systems and transducers. Rockville, MD: FDA (2008).
189. O'Brien WD Jr. Ultrasound-biophysics mechanisms. *Prog Biophys Mol Biol* 93, 212–255 (2007). [PubMed: 16934858]
190. Bushberg JT & Boone JM *The essential physics of medical imaging*. (Lippincott Williams & Wilkins, 2011).
191. Nelson TR, Fowlkes JB, Abramowicz JS & Church C.C.J.J.o.u.i.m. Ultrasound biosafety considerations for the practicing sonographer and sonologist. 28, 139–150 (2009).
192. Hinchet R et al. Transcutaneous ultrasound energy harvesting using capacitive triboelectric technology. *Science* 365, 491 (2019). [PubMed: 31371614]
193. Samineni VK et al. Fully implantable, battery-free wireless optoelectronic devices for spinal optogenetics. *Pain* 158, 2108–2116 (2017). [PubMed: 28700536]
194. Harvey CD, Collman F, Dombbeck DA & Tank DW Intracellular dynamics of hippocampal place cells during virtual navigation. *Nature* 461, 941–946 (2009). [PubMed: 19829374]
195. Tye KM et al. Amygdala circuitry mediating reversible and bidirectional control of anxiety. *Nature* 471, 358–362 (2011). [PubMed: 21389985]
196. Yilmaz G & Dehollain C *Wireless power transfer and data communication for neural implants: case study: epilepsy monitoring*. (Springer, 2017).
197. Liang T & Yuan YJ *Wearable Medical Monitoring Systems Based on Wireless Networks: A Review*. *Ieee Sens J* 16, 8186–8199 (2016).
198. Zhang ZH, Russell LE, Packer AM, Gauld OM & Hausser M Closed-loop all-optical interrogation of neural circuits in vivo. *Nature Methods* 15, 1037–1040 (2018). [PubMed: 30420686]
199. Mirza KB, Golden CT, Nikolic K & Toumazou C Closed-Loop Implantable Therapeutic Neuromodulation Systems Based on Neurochemical Monitoring. *Front Neurosci-Switz* 13 (2019).
200. Jun JJ et al. Fully integrated silicon probes for high-density recording of neural activity. *Nature* 551, 232 (2017). [PubMed: 29120427]
201. Aravanis AM et al. An optical neural interface: in vivo control of rodent motor cortex with integrated fiberoptic and optogenetic technology. *J. Neural Eng* 4, S143–S156 (2007). [PubMed: 17873414]
202. Shin Y et al. Characterization of fiber-optic light delivery and light-induced temperature changes in a rodent brain for precise optogenetic neuromodulation. *Biomed. Opt. Express* 7, 4450–4471 (2016). [PubMed: 27895987]
203. Wang Z, Hu M, Ai X, Zhang Z & Xing B Near-infrared manipulation of membrane ion channels via upconversion optogenetics. *Adv. Biosyst* 3 (2018).
204. Lin JY, Knutsen PM, Muller A, Kleinfeld D & Tsien RY ReaChR: a red-shifted variant of channelrhodopsin enables deep transcranial optogenetic excitation. *Nat. Neurosci* 16, 1499–1508 (2013). [PubMed: 23995068]
205. Arrenberg AB, Bene FD & Baier H Optical control of zebrafish behavior with halorhodopsin. *Proc. Natl. Acad. Sci. USA* 106, 17968–17973 (2009). [PubMed: 19805086]
206. Yarmolenko PS et al. Thresholds for thermal damage to normal tissues: an update. *Int. J. Hyperthermia* 27, 320–343 (2011). [PubMed: 21591897]

207. Goncalves SB et al. LED optrode with integrated temperature sensing for optogenetics. *Micromachines* 9, 473 (2018). [PubMed: 30424406]
208. Khan W et al. Inductively coupled, mm-sized, single channel optical neuro-stimulator with intensity enhancer. *Microsyst. Nanoeng* 5, 23 (2019). [PubMed: 31231537]
209. Kampasi K et al. Fiberless multicolor neural optoelectrode for in vivo circuit analysis. *Sci Rep* 6, 30961 (2016). [PubMed: 27485264]
210. Samineni VK et al. Optogenetic silencing of nociceptive primary afferents reduces evoked and ongoing bladder pain. *Sci. Rep* 7, 15865 (2017). [PubMed: 29158567]
211. Busskamp V & Roska B Optogenetic approaches to restoring visual function in retinitis pigmentosa. *Curr. Opin. Neurobiol.* 21, 942–946 (2011). [PubMed: 21708457]
212. Busskamp V, Picaud S, Sahel JA & Roska B Optogenetic therapy for retinitis pigmentosa. *Gene Ther* 19, 169–175 (2012). [PubMed: 21993174]
213. Chow BY & Boyden ES Optogenetics and translational medicine. *Sci. Transl. Med* 5, 177ps175 (2013).
214. Krook-Magnuson E, Armstrong C, Oijala M & Soltesz I On-demand optogenetic control of spontaneous seizures in temporal lobe epilepsy. *Nat. Commun* 4, 1376 (2013). [PubMed: 23340416]
215. Paz JT et al. Closed-loop optogenetic control of thalamus as a tool for interrupting seizures after cortical injury. *Nat. Neurosci* 16, 64–70 (2013). [PubMed: 23143518]
216. Nussinovitch U & Gepstein L Optogenetics for in vivo cardiac pacing and resynchronization therapies. *Nat. Biotechnol* 33, 750–754 (2015). [PubMed: 26098449]
217. Shao J et al. Smartphone-controlled optogenetically engineered cells enable semiautomatic glucose homeostasis in diabetic mice. *9, eaal2298* (2017).
218. Bansal A, Yang F, Xi T, Zhang Y & Ho JS In vivo wireless photonic photodynamic therapy. *Proc. Natl. Acad. Sci. USA* 115, 1469–1474 (2018). [PubMed: 29378941]
219. Kramer RH, Mouroto A & Adesnik H Optogenetic pharmacology for control of native neuronal signaling proteins. *Nat. Neurosci* 16, 816–823 (2013). [PubMed: 23799474]
220. Banghart MR & Sabatini BL Photoactivatable neuropeptides for spatiotemporally precise delivery of opioids in neural tissue. *Neuron* 73, 249–259 (2012). [PubMed: 22284180]
221. Jennings JH et al. Distinct extended amygdala circuits for divergent motivational states. *Nature* 496, 224–228 (2013). [PubMed: 23515155]
222. Stamatakis AM et al. A unique population of ventral tegmental area neurons inhibits the lateral habenula to promote reward. *Neuron* 80, 1039–1053 (2013). [PubMed: 24267654]
223. McCall JG et al. CRH engagement of the locus coeruleus noradrenergic system mediates stress-induced anxiety. *Neuron* 87, 605–620 (2015). [PubMed: 26212712]
224. McCall JG et al. Preparation and implementation of optofluidic neural probes for in vivo wireless pharmacology and optogenetics. *Nat. Protoc* 12, 219–237 (2017). [PubMed: 28055036]
225. Creed M, Pascoli VJ & Lüscher C Refining deep brain stimulation to emulate optogenetic treatment of synaptic pathology. *Science* 347, 659–664 (2015). [PubMed: 25657248]
226. McCall JG & Jeong JW Minimally invasive probes for programmed microfluidic delivery of molecules in vivo. *Curr. Opin. Neurobiol* 36, 78–85 (2017).
227. Noh KN et al. Miniaturized, battery-free optofluidic systems with potential for wireless pharmacology and optogenetics. *Small* 14, 1702479 (2018).
228. Shmuel A, Augath M, Oeltermann A & Logothetis NK Negative functional MRI response correlates with decreases in neuronal activity in monkey visual area V1. *Nat. Neurosci* 9, 569–577 (2006). [PubMed: 16547508]
229. Liu JN, Bu W & Shi J Chemical design and synthesis of functionalized probes for imaging and treating tumor hypoxia. *Chem. Rev* 117, 6160–6224 (2017). [PubMed: 28426202]
230. Hopf HW & Rollins MD Wounds: an overview of the role of oxygen. *Antioxid. Redox Signal* 9, 1183–1192 (2007). [PubMed: 17536961]
231. Neely RM, Piech DK, Santacruz SR, Maharbiz MM & Carmena JM Recent advances in neural dust: towards a neural interface platform. *Curr. Opin. Neurobiol* 50, 64–71 (2018). [PubMed: 29331738]

232. Ghanbari MM, Piech DK, Shen K, Alamouti SF, Yalcin C, Johnson BC, Carmena JM, Maharbiz MM and Muller R, 2019. A Sub-mm 3 Ultrasonic Free-Floating Implant for Multi-Mote Neural Recording. *IEEE Journal of Solid-State Circuits*, 54, 3017–3030 (2019).
233. Ghanbari MM, Piech DK, Shen K, Alamouti SF, Yalcin C, Johnson BC, Carmena JM, Maharbiz MM and Muller R A 0.8 mm 3 Ultrasonic Implantable Wireless Neural Recording System With Linear AM Backscattering. In 2019 IEEE International Solid-State Circuits Conference-(ISSCC), pp. 284–286 (2019).
234. Kang SK, Koo J, Lee YK & Rogers JA Advanced materials and devices for bioresorbable electronics. *Acc Chem Res* 51, 988–998 (2018). [PubMed: 29664613]
235. Won SM et al. Natural wax for transient electronics. *Adv. Funct. Mater* 28 (2018).
236. Boutry CM et al. Biodegradable and flexible arterial-pulse sensor for the wireless monitoring of blood flow. *Nat Biomed Eng* 3, 47–57 (2019). [PubMed: 30932072]
237. Koo J et al. Wireless bioresorbable electronic system enables sustained nonpharmacological neuroregenerative therapy. *Nat. Med* 24, 1830–1836 (2018). [PubMed: 30297910]
238. Son D et al. Bioresorbable electronic stent integrated with therapeutic nanoparticles for endovascular diseases. *ACS Nano* 9, 5937–5946. [PubMed: 25905457]
239. Pashaie R et al. Closed-loop optogenetic brain Interface. *IEEE Trans. Biomed. Eng* 62, 2327–2337 (2015). [PubMed: 26011877]
240. Jonsson A et al. Bioelectronic neural pixel: Chemical stimulation and electrical sensing at the same site. *Proc Natl Acad Sci U S A* 113, 9440–9445 (2016). [PubMed: 27506784]
241. Capogrosso M et al. A brain-spine interface alleviating gait deficits after spinal cord injury in primates. *Nature* 539, 284–288 (2016). [PubMed: 27830790]
242. Zanos S Closed-Loop Neuromodulation in Physiological and Translational Research. *Cold Spring Harb Perspect Med* 9 (2019).
243. Lo MC & Widge AS Closed-loop neuromodulation systems: next-generation treatments for psychiatric illness. *Int Rev Psychiatry* 29, 191–204 (2017). [PubMed: 28523978]
244. Yamagishi K et al. Tissue-adhesive wirelessly powered optoelectronic device for metronomic photodynamic cancer therapy. *Nat. Biomed. Eng* 3, 27–36 (2019) [PubMed: 30932063]

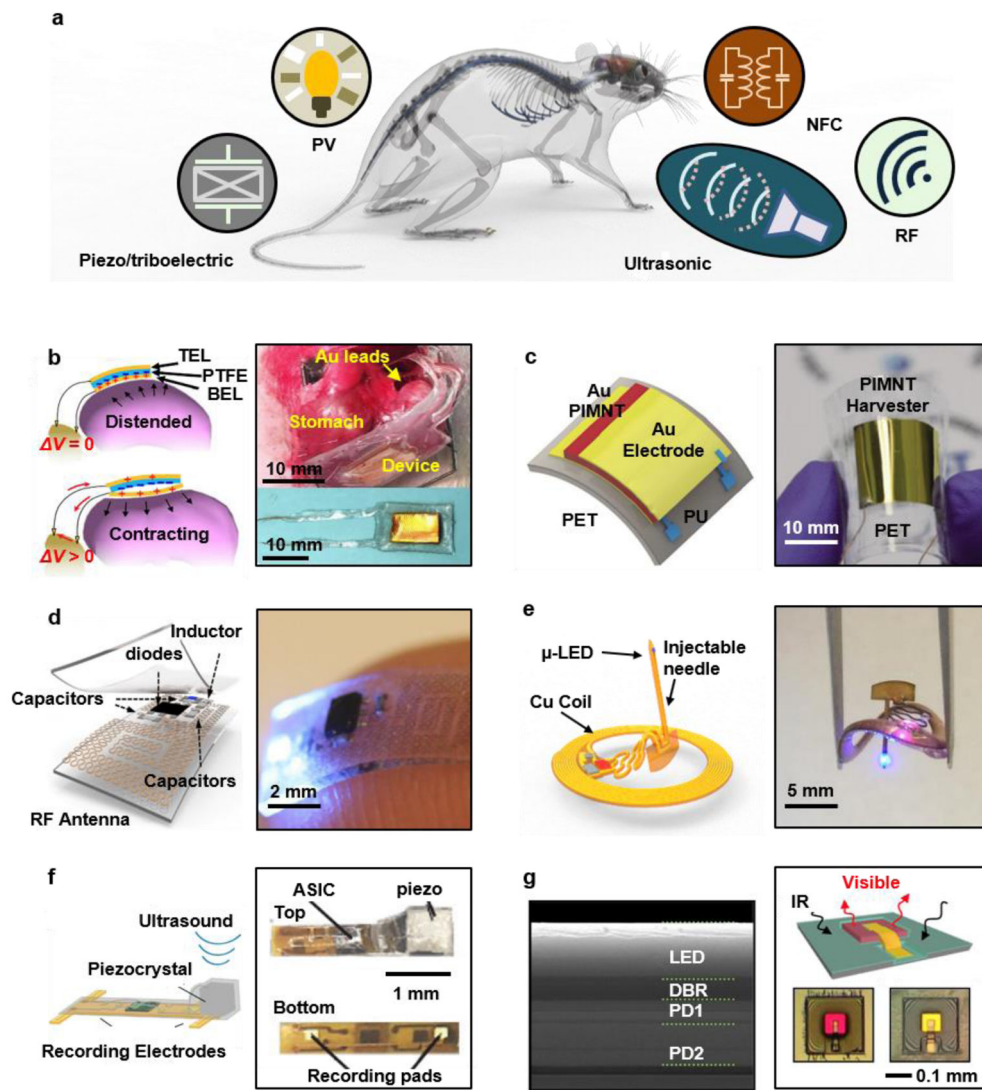




**Figure 1. Wireless technologies in implantable electronics.**

**a**, Schematic illustration of fully implantable wireless interfaces to the central nervous system (CNS), spinal cord and peripheral nervous system (PNS), with functional options in electronic/optogenetic recording/stimulation and microfluidic drug delivery. **b**, A mouse with wireless devices implanted near the spinal cord while running on a wheel. Reproduced from Ref.<sup>98</sup> Copyright 2015 Springer Nature. **c**, Direct experimental data on wireless and tethered electronic implants that highlight the advantages of the former in studying social interactions and total activity levels of mice in open field arenas. Reproduced from Ref.<sup>60</sup> Copyright 2018 National Academy of Sciences. **d**, Examples of miniaturized wireless implantable electronic systems for *in-vivo* physiological recording and neural stimulation in various animal models, including fish, mice, birds and monkeys. Reproduced from Ref.<sup>64, 67</sup> Copyright 2006, 2009 Elsevier.





**Figure 2. Strategies for power supply in wireless, battery-free implantable devices.**  
**a.** Schematic illustration of power harvesting and delivery strategies, including photovoltaic (PV), near-field magnetic resonance coupling, radio frequency power transfer (far-field), ultrasonic and ambient mechanical (piezoelectric and triboelectric) power harvesting. **b.** Autonomous devices that provide electrical stimulation to the vagus nerve for weight control, with power supplied by a triboelectric generator that harvests mechanical energy from movements of the stomach. Reproduced from Ref.<sup>119</sup> Copyright 2018 Springer Nature. **c.** Flexible piezoelectric energy harvester for powering a deep brain stimulator. Reproduced from Ref.<sup>118</sup> Copyright 2015 Royal Society of Chemistry. **d.** Soft, stretchable and fully implantable wireless optogenetic stimulator powered by far-field RF power transfer. Reproduced from Ref.<sup>98</sup> Copyright 2015 Springer Nature. **e.** Fully implantable, wireless optogenetic deep brain stimulator powered by magnetic resonant coupling. Reproduced from Ref.<sup>100</sup> Copyright 2017 Cell Press. **f.** Electrophysiological recording device powered by ultrasound. Reproduced from Ref.<sup>126</sup> Copyright 2016 Cell Press. **g.** Implantable

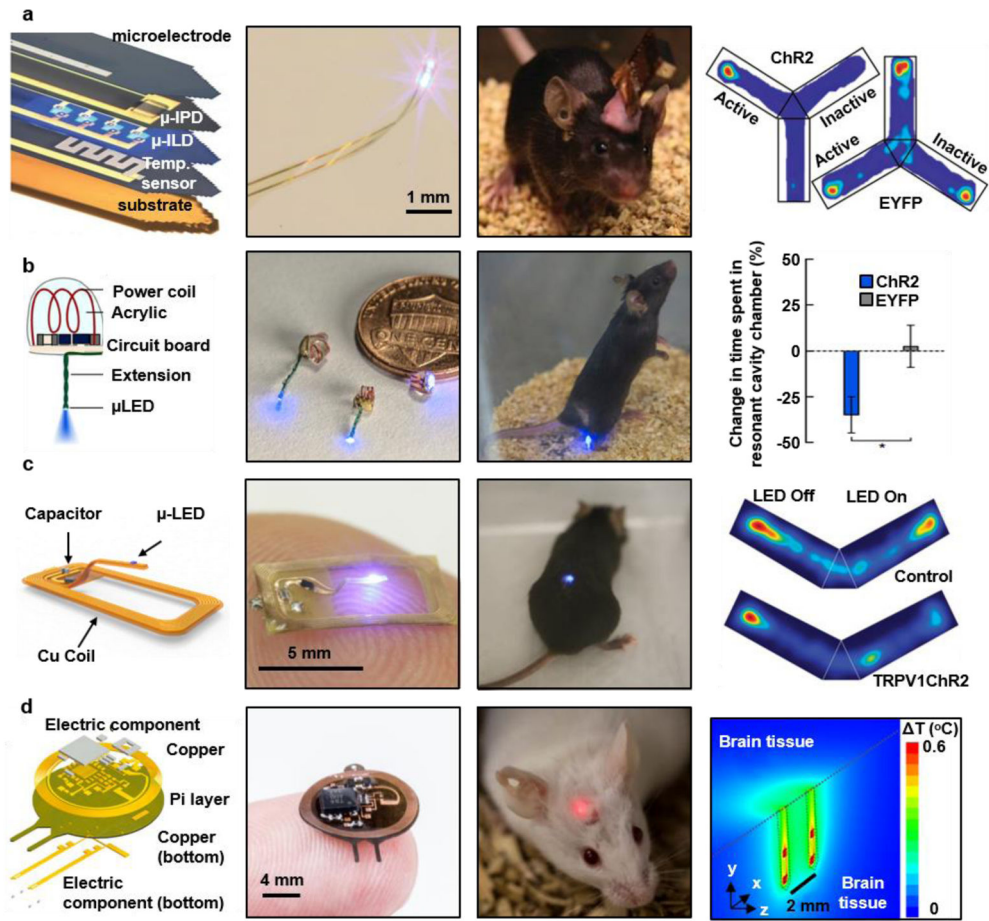
microscale optoelectronic neuromodulator powered by infrared light. Reproduced from Ref.<sup>124</sup> Copyright 2018 National Academy of Sciences.

Author Manuscript

Author Manuscript

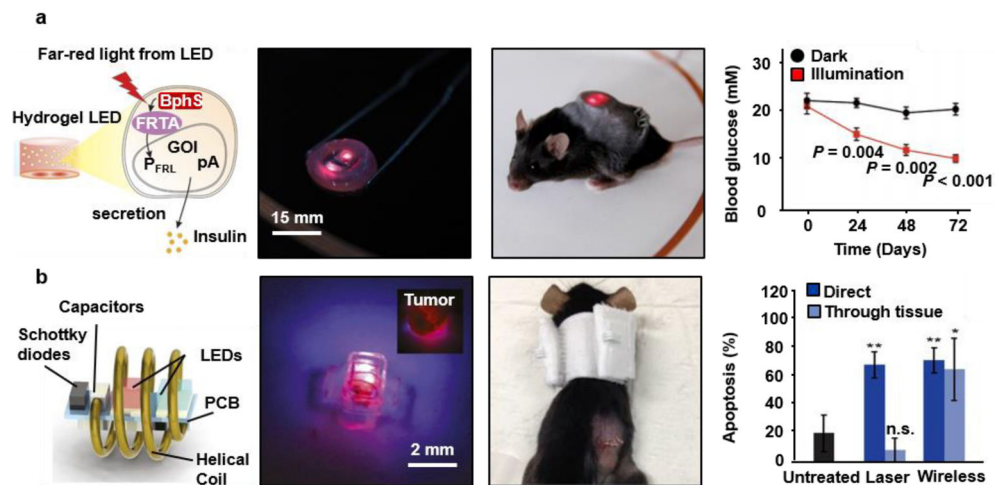
Author Manuscript

Author Manuscript



**Figure 3. Optogenetic interfaces to regulate cell activity.**

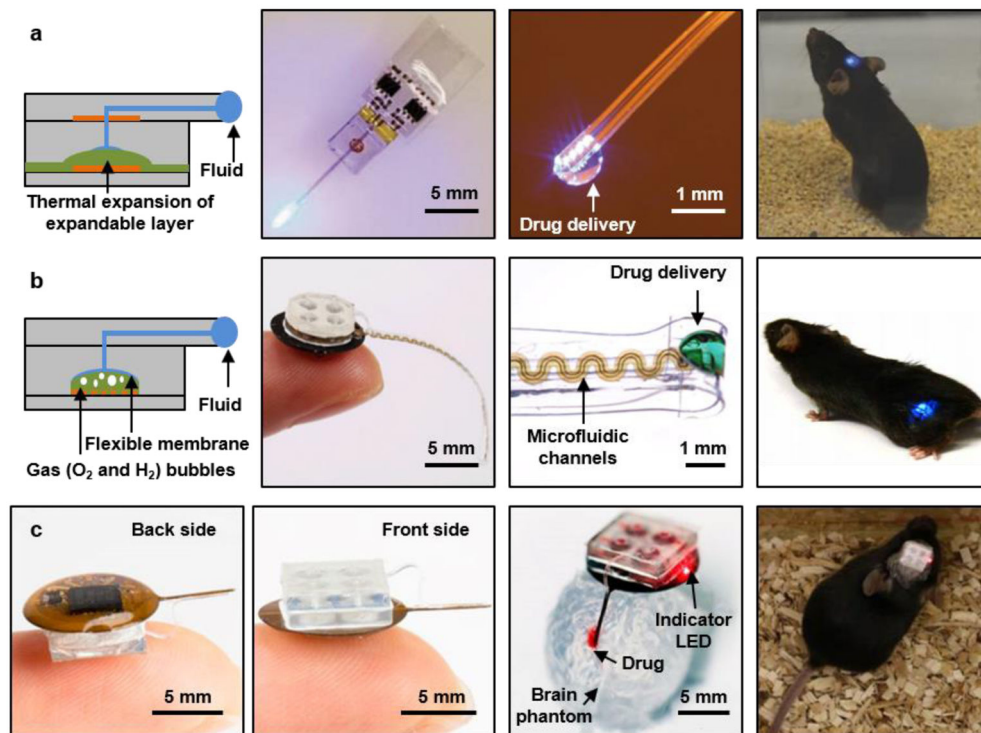
**a**, Injectable probe for optogenetic stimulation, electrical recording, temperature sensing, and photometry. Reproduced from Ref.<sup>99</sup> Copyright 2013 American Association for the Advancement of Science (AAAS). **b**, Miniaturized implantable optogenetic probes powered by an RF generator and a resonant cavity for neuromodulation in the brain, spinal cord, and peripheral nervous system. Reproduced from Ref.<sup>122</sup> Copyright 2015 Springer Nature. **c**, Optogenetic probe in a thin and flexible open architecture, powered by near-field magnetic resonant coupling for long-term use in the spinal cord. Reproduced from Ref.<sup>100</sup> Copyright 2017 Lippincott Williams & Wilkins. **d**, Implantable optoelectronic system consisting of four  $\mu$ LEDs on two bilateral probes and an integrated circuit for stable multimodal interfaces during chronic operation. Reproduced from Ref.<sup>102</sup> Copyright 2018 Springer Nature.



**Figure 4. Implantable and wireless devices for photonic therapy.**

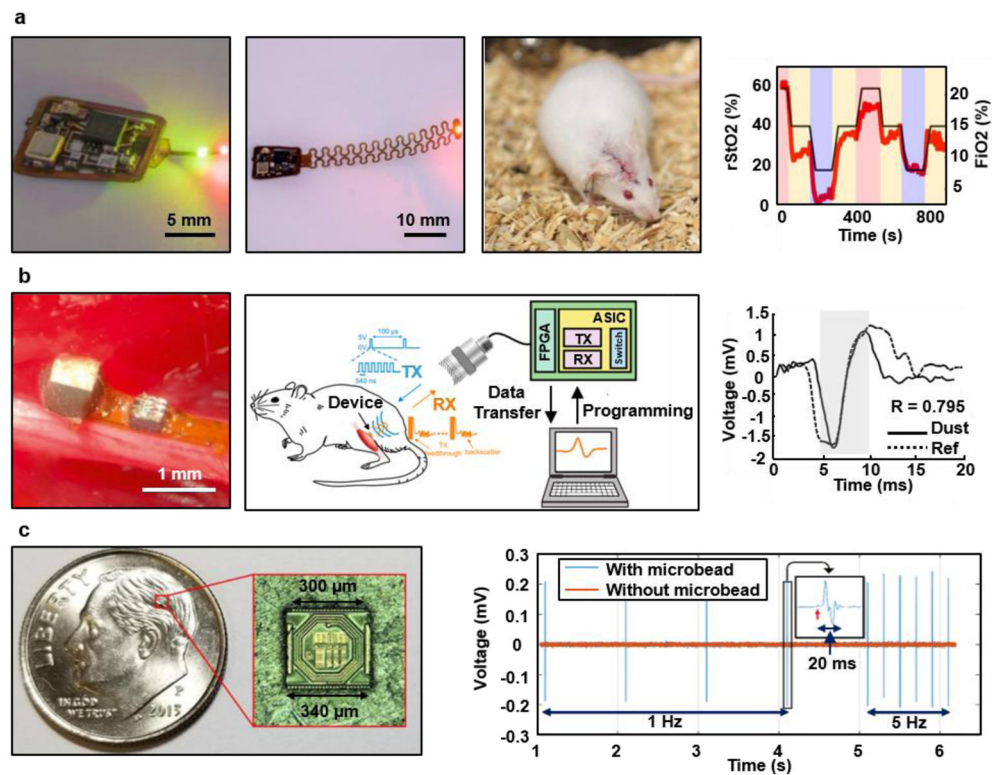
**a**, Optogenetic stimulation system for remotely controlling the release of glucose-lowering hormones from optically engineered cells in diabetic mice. Ref.<sup>217</sup> Copyright 2017

American Association for the Advancement of Science (AAAS). **b**, An optoelectronic device wirelessly powered with RF radiation for photodynamic therapy at the target site, where the system modulates the light emission for optimum therapeutic dosage. Reproduced from Ref.<sup>218</sup> Copyright 2018 National Academy of Sciences.



**Figure 5. Wireless systems for programmed microfluidic delivery of pharmacological agents.** **a**, Optofluidic probe and thermally actuated pumps that combine Joule heating elements as actuators and thermally expandable materials as mechanical transducers, all integrated with an RF powered wireless module and microcontroller for independent fluid delivery from four separate chambers to regions of the deep brain. Reproduced from Ref.<sup>227</sup> Copyright 2017 Wiley-VCH Verlag. **b**, Optofluidic cuff system and electrochemical pump for the programmed delivery of light and pharmacological agents to peripheral nerves. Reproduced from Ref.<sup>144</sup> Copyright 2019 American Association for the Advancement of Science (AAAS). **c**, Injectable microsystems for programmable optogenetics and pharmacology at targeted areas of deep brain. Reproduced from Ref.<sup>62</sup> Copyright 2019 National Academy of Sciences.

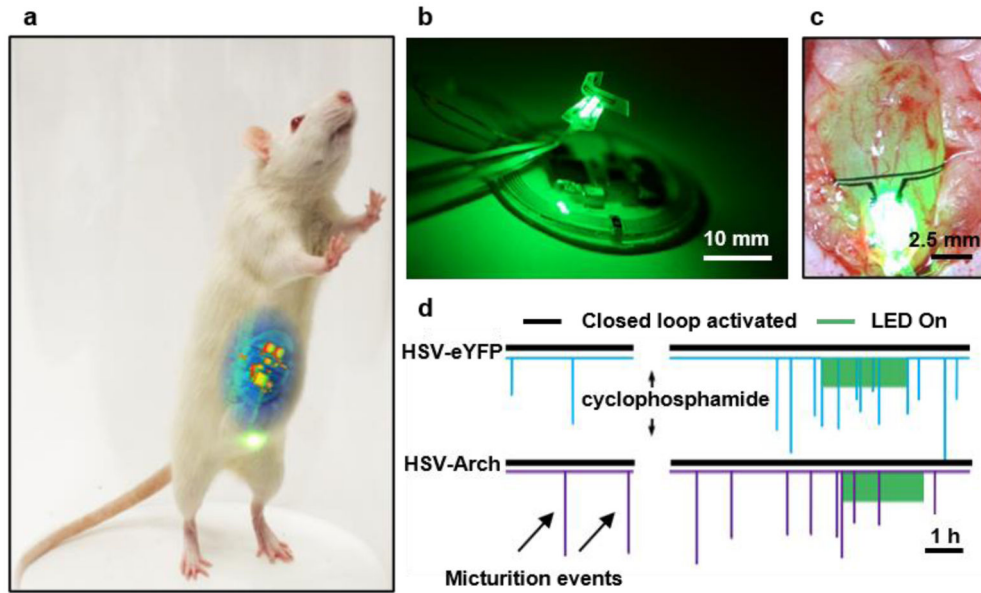




**Figure 6. Wireless systems for biosignal recording.**

**a**, Wireless optoelectronic system for continuously monitoring regional tissue oxygenation ( $rStO_2$ ) at sites of interest such as peripheral tissues and the deep brain. Reproduced from Ref.<sup>143</sup> Copyright 2019 American Association for the Advancement of Science (AAAS).  
**b**, An ultrasound-based device for measuring electromyograms and electroneurograms from the gastrocnemius muscle and sciatic nerve, respectively. Reproduced from Ref.<sup>126</sup> Copyright 2016 Cell Press. **c**, Miniaturized neural interface based on a 130 nm CMOS fabrication process for neural recording and bipolar stimulation of the sciatic nerves. Reproduced from Ref.<sup>146</sup> Copyright 2019 Institute of Electrical and Electronics Engineers.






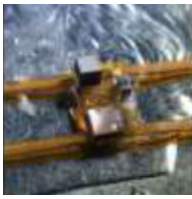




**Figure 7. Fully implantable, wireless, battery-free system for automated, closed-loop peripheral neuromodulation.**

**a**, A rat with an implanted device during activation of the  $\mu$ LEDs. **b**, A device that combines a wireless control/power management module, an optical sensing/stimulation module and a wireless power transfer module. **c**, Optical image of a strain gauge and  $\mu$ LEDs wrapped around the bladder of a rat in an expanded state. **d**, Result of closed-loop optogenetic neuromodulation. Reproduced from Ref.<sup>141</sup> Copyright 2019 Springer Nature.

**Table 1.**  
**Summary of device architectures for wireless, battery-free operation of fully implantable stimulation and recording tools for the central nervous system.**

EM, electromagnetic; RF, radio-frequency; SAR, specific absorption rate; RX, receiving; BL, Bluetooth; PV, photovoltaic; US, ultrasonic. Reproduced from Ref.<sup>98, 100, 134, 141, 149, 158, 184</sup>

Summary of operational modes for wireless, battery-free implantable devices						
Power source		Features		Example		Reference
External power source	EM	Far field, passive	Weight: 16-33 mg Available power: ~ 3-5 mW Operational distance: 0.1-3 m Tissue impact: SAR 6150-69 mW/kg	Downlink: RF Uplink: N/A Control: Analog, multi-band RX antenna Embodiment: Subdermal Application: Deep brain/spinal cord/peripheral neural stimulation		98, 101, 122
		Near to mid field, Magnetic resonant coupling	Weight: ~ 30 mg Available power: ~ 5-10 mW Operational distance: 0.1-1m Tissue impact: SAR ~ < 20 mW/kg	Downlink: RF Uplink: N/A Control: Digital, active Embodiment: Subdermal Application: Brain optogenetics, local oximetry, microfluidic drug delivery		100, 102, 145, 193
		PV	Weight: 11 μg – 70 mg Available power: 45 μW – 7 mW Operational distance: ~ 0.5 m Tissue impact: heating of 5 °C with 250-300 mW/mm <sup>2</sup> IR radiation for 20 min	Downlink: light (green) Uplink: light (red) Control: Digital Embodiment: N/A Application: Brain neural recording		123, 124, 142, 158,
		US	Weight: 7.6 mg Available power: 0.12 mW Operational distance: ~ 10 cm in tissue, direct body-transducer contact (transducer in contact with body) Tissue impact: local rate of heat generation ~0.3 – 240 mWcm <sup>-3</sup> (soft tissue); ~ 8 – 6000 mWcm <sup>-3</sup> (bone); ~ 15 – 12000 mW cm <sup>-3</sup> (lung)	Downlink: US Uplink: US Control: N/A Embodiment: Deep in tissue / on nerve Application: Physiological/neural recording		125, 126, 184
Internal power source	Triboelectric	Available power: ~ 0.26 mW (peak) Operational distance: N/A	Downlink: N/A Uplink: N/A Control: N/A Embodiment: on organ/ nerve Application: Self-triggered electrical neural stimulation		118, 119, 134	

Summary of operational modes for wireless, battery-free implantable devices					
Power source		Features	Example		Reference
	Biofuel	Available power: ~ $\mu$ W Operational distance: N/A Tissue impact: Biofouling, inflammation	Downlink: RF Uplink: Bluetooth Control: Digital Embodiment: Application: Implantable biofuel cell		136, 149

Author Manuscript

Author Manuscript

Author Manuscript

Author Manuscript

**Table 2.**

Power consumption for various modalities.

Operation modality	Power consumption
Electrical recording	9 $\mu\text{W}/\text{ch}$ <sup>127</sup> , 3.37 $\mu\text{W}/\text{ch}$ <sup>128</sup> , 16 nW <sup>129</sup> , 906 $\mu\text{W}/\text{ch}$ <sup>34</sup> , 8 $\mu\text{W}/\text{ch}$ <sup>61</sup> , 2 mW/ch <sup>130</sup>
Optical recording	10 mW (peak) and 2 mW (ave.) <sup>143</sup> , 10.37 mW (active) and 119 $\mu\text{W}$ (sleep) <sup>131</sup> , < 15 mW (continuous) <sup>60</sup>
Electrical stimulation	21.4 mW (peak), 1.8 mW (ave.) (30 Hz, 0.8% duty cycle) <sup>132</sup> , < 40 $\mu\text{W}$ <sup>119</sup>
Optogenetic stimulation	2 – 10 mW (continuous mode, depending on light intensity) <sup>100, 122</sup>
Pharmacological stimulation	1.3 mW (average, 86% duty cycled) <sup>62</sup>

Author Manuscript

Author Manuscript

Author Manuscript

Author Manuscript